CALIFORNIA STATE UNIVERSITY, NORTHRIDGE

The Identification of a Novel Cripto/MyosinII Interaction that Promotes Stem Cell-Mediated Tissue Regeneration

A thesis submitted in partial fulfillment of the requirements
For the degree of Master of Science in Biology

By
Malachia Yvonne Hoover

May 2017

The thesis of Malachia Yvonne Hoover is approved by:

_____ _____
Dr. Lisa Banner Date

_____ _____
Dr. Maria Elena de Bellard Date

_____ _____
Dr. Jonathan Kelber, Chair Date

California State University, Northridge

Acknowledgements

I would like to first acknowledge the faculty and administration at California State University, Northridge, for the great amount of assistance they've provided me throughout my Master's career. The Department of Biology, the College of Math and Science, and Graduate Studies, and the Research Initiative for Scientific Enhancement (RISE) at CSUN have granted me numerous scholarships and awards that have assisted towards my thesis project and school tuition. The RISE program played an influential part in my success at CSUN. The financial support and professional development skills I received from RISE and the program director, Dr. Zavala, allowed me to focus and excel on my research project and polish my application packet for Ph.D. interviews. Thank you also to Parthenia Hosch and Julie Doubt for the administrative work they conduct for the RISE program. I would also like to thank Dr. Bill Kromer and Marc Felix for helping with any and all technical support and maintenance for our lab. Special thanks also to Toni Uhlendorf and Fritz Hertel for helping tremendously with the husbandry of our zebrafish in the vivarium.

Next, I want to thank my present and past lab members for their valuable support and friendship, including: Yvess Adamian, Sa La Kim, Megan Agajanian, Justin Molnar, Preston Shisgal, Kayla Meade, Sarkis Hamalian, Julie Hong, Erika Duell, Brandon Wallace, Daniel Brambilla, Laurelin Wolfenden, Anaamika Campeau, Alexander Hou, Anjelica Cardenas, Homa Hemmati, Farhana Runa, Gabriela Alvarez, Lindsay Kutscher, Bryant Oliva, and Caroline Arellano-Garcia. I would like to especially thank my undergraduate trainee, Erika Duell, for all the tenuous work you dedicated towards our project. Throughout this journey, my lab members have given me immense support both

academically and personally and have become a second family to me. It has been a pleasure to work with such a motivated and charismatic group of researchers.

Thank you to my committee members, Dr. Maria Elena de Bellard, Dr. Lisa Banner, and my Principal Investigator (PI), Dr. Jonathan Kelber, for the counsel and direction provided towards my thesis project. I would also like to additionally thank Dr. de Bellard for allowing me to use her Leica microscope for my fish imaging.

Finally, I would like to give special appreciation to my PI, Dr. Kelber, for pushing me to reach my highest capabilities as a scientist. Dr. Kelber has equipped me with not only with the molecular and cellular techniques in the field of biomedical sciences, but the capability to critically think as a researcher. Although a state institution, our lab conducts novel breakthrough science on the level of larger institutions and was recently funded a prestigious SC1 grant from the National Institute of Health (NIH). It is such training that has enabled me admittance to Stanford University's Ph.D. program in Stem Cell and Regenerative Medicine. I am highly thankful for the guidance and mentorship you've given me – you are truly a great PI and mentor.

Dedication

My thesis work is dedicated to my family who has supported me throughout my entire life. To my mother, thank you for always giving me the best encouragement and for telling me how great I am. To hear that constantly as I child, you engrained within a passion to excel. Despite the socioeconomic disparities we faced as a family, your strength and perseverance has showed me just how powerful the African American woman can be in our society. You never gave up, and I am so proud that you are pursuing a Ph.D. in Public Administration because we need more African American principals and teachers - you are truly my role model. To my father, you are a survivor and despite suffering a stroke and having diabetes since a child, you continue to persist. My passion for discovering novel stem cell treatments for regenerative purposes is inspired by you! I want to find a cure that could potentially better your livelihood and others like you – that is my mission in life. To my younger three sisters and brother, I hope my work can encourage you all to be great professionals in which ever field you individually aspire to pursue. I want to be the best role model for you all, and remember that your big sister will always be there for you all, despite the fact we're divided between two continents. This work is also dedicated to my little niece and nephew, Aisha and Ibrahim. You two are the next generation and I see so much hope and life in both your innocent eyes. Also, thank you to my grandmother, all my aunts and uncles, and cousins. I have the best family in the world. Lastly, I dedicate this work to my fiancée and soon to be husband, Jesse Cudjoe. Thank you for always being my ultimate supporter and for comforting me during the times I thought I reached my breaking point. You are so compassionate and loving, and I am so happy to have you in my life. I couldn't have done this without you, love.

Table of Contents

List of Figures

List of Tables

Abstract

Identification of a Novel Cripto/Myosin II Interaction that Promotes Stem Cell-Mediated Tissue Regeneration

By

Malachia Yvonne Hoover

Master of Science in Biology

Stem cells are necessary for proper development, tissue homeostasis and regeneration while dysregulation of their activity leads to diseases such as diabetes, neurodegeneration and cancer. Yet, the molecular and cellular mechanisms that drive stem cell mediated regeneration remain to be fully elucidated. We hypothesized that the stem cell marker, Cripto (or TDGF1), is a regulator of tissue regeneration. Using the zebrafish model of caudal fin wound healing, we show that expression of the zebrafish Cripto homolog, one-eyed pinhead (or oep), is increased at 96 hours post amputation within a previously established window of stem cell enrichment in this model. We further demonstrate that Cripto is necessary and sufficient for stem cell mediated regeneration in this *in vivo* model as well as in an *in vitro* wound healing assay. We identified non-muscle myosin II's (MYH9/10) as novel Cripto binding proteins using co-immunoprecipitation (Co-IP) and mass spectrometry and confirmed the interaction between these proteins via Co-IP/Western blot from mammary epithelial cells and endogenous immunofluorescence co-localization in mesenchymal stem cells, a key cell type that contributes to wound healing in zebrafish and mammals. Notably, the effects of Cripto and MYH9/10 inhibitors on regeneration of wounded zebrafish caudal fins were not additive suggesting Cripto and MYH9/10 have overlapping functions and mechanisms of action. Cripto and its homologs are cell-surface GPI-anchored

glycoproteins that can be released via GPI anchor cleavage by phospholipases. We previously demonstrated that tissue-specific stem cell functions of Cripto depend upon its soluble secreted form and this led us to test whether MYH9/10 function may be required for transporting Cripto to the cell surface or mediating release of soluble Cripto from the cell surface. Indeed, we find that cell-surface localization of Cripto in and its release as a soluble factor from mammalian cells requires MYH9/10 function. Using Bio-Grid proteomics, we discovered Rab11A, an endosomal and exosomal marker, to be a co-binder of GRP78 and Myosin IIs. We then pharmacologically inhibited Myosin IIs using Blebbistatin or Rho Kinase (ROCK) inhibitors in mesenchymal stem cells transfected with wild-type, constitutively active, and dominant negative Rab11A constructs. Our results show that the expression of Rab11A regulates Cripto and Myosin II binding interactions, suggesting a possible role for Rab11A in the endosomal and exosomal trafficking of Cripto. Based on our findings, we propose a new model whereby MYH9/10/Rab11A-mediated Cripto transport enables cells to generate a pool of extracellular Cripto that can subsequently function in autocrine and/or paracrine pathways to promote stem cell mediated regeneration and wound healing.

Chapter 1: Introduction

An organism's ability to restore and renew tissue and organs is an essential process needed for normal homeostasis and wound healing. In response to injury, tissue repair can occur either by complete or limited regeneration. Restitution of the normal structure is defined as tissue regeneration, but in humans, this process is often incomplete. Although humans possess the ability to regenerate some structures including the skin, pancreas, and gut epithelium, their regenerative capacity, like that of most mammals, is relatively limited [1-4]. At the expense of complete regeneration, wound healing is often favored by which the normal architecture of the tissue is permanently altered by the formation of a scar. The bulk of the scar consists of disorganized extracellular matrix proteins (primarily collagen) and necrotic cells (primarily fibroblasts). The fibrotic scar not only disrupts the structure of the tissue, but also its activity and functionality. In diseases such as diabetes and myocardial infarction, the tissue's inability to fully regenerate back to its normal state leads to disease progression and ultimately death [5,6]. Therefore, it is critical to understand the cellular and molecular mechanism governing regeneration and wound healing in hopes for the development of novel therapeutics to treat such degenerative diseases.

In contrast to mammals, other vertebrate organisms such as the *Danio rerio* or zebrafish, have a greater regenerative capacity to heal damaged organs and tissues like the heart, fin, retina, optic nerve, liver, spinal cord and sensory hair cells without the by-product of a scar [7-12]. Exploring why some organisms possess a better ability to regenerate over others is a pertinent question in research that can provide insight towards potential mechanisms of improving wound healing in humans. Therefore, the zebrafish

serve as a remarkable model system to study this process of regeneration. In particular, the zebrafish caudal fin is a powerful tool to study regeneration due to its accessibility, simple architecture, and its robust and fast capacity to regenerate. This process involves the complete restoration of bone, epidermis, blood vessels, nerves, connective tissue and pigmentation that is completed in approximately 3 days in larval fish and 2 weeks in adult fish [13]. When the caudal fin is amputated in the adult, 24 hours post amputation (hpa) the wound is initially closed off by non-proliferative epithelial cells that migrate to the wound site and form the apical epidermal cap (AEC). From 24-96 hpa, the mesenchymal tissue underneath the AEC loses cellular organization and the cells begin to dedifferentiate into progenitor cells and migrate towards the site of injury to form the blastema. The blastemal is a highly proliferative mass of mesenchymal stem cells that proliferate to give rise to new tissue [14]. By one week, the stem cells continue to proliferate during which bone is deposited and properly patterned [15]. Within 10-15 days post amputation (dpa), the blastema continues to grow and the remainder of differentiated cell types is formed to collectively give rise to a new fin.

Shown in both mammalian and fish systems, a pivotal component of the regenerative process is the presence of mesenchymal stem cells (MSCs). MSCs are subpopulation of stem cells that can differentiate into lineage-specific connective tissue cell types, including osteoblasts, chondrocytes, myocytes, adipocytes, and fibroblasts. MSCs are involved in all three stages of the wound healing process, which include the inflammation, proliferation, and remodeling phases. Studies have shown that the addition of MSCs decreases the immune cell secretion of pro-inflammatory cytokines, TNF-α and interferon-γ, while increasing the production of anti-inflammatory cytokines, interleukin-

10 (IL-10) and IL-4 [16]. MSCs also promote angiogenesis, and induce cell migration and proliferation of keratinocytes, dermal fibroblasts, and host stem cells during the proliferative phase by the secretion of soluble factors [17,18]. Importantly, MCSs possess anti-scarring properties and secrete factors such as matrix metalloproteinases (MMPs) that degrade the extracellular matrixes and also promote the organization of ECM deposition to reduce the amount of scarring in the remodeling phase [19]. Overall, MSCs enhance tissue regeneration and wound healing, yet dysregulation of their activity can lead to not only improper wound healing but also disease such as diabetes and cancer.

In this regard, Cripto or teratocarcinoma-derived growth factor (TDGF1) is a GPI-linked cell surface molecule known to regulate key biological functions including cell migration and proliferation, epithelial-to-mesenchymal transition, and importantly, stem cell maintenance and self-renewal. It is the founding member of the epidermal growth factor (EGF)-Cripto-1-FRL-1-Cryptic (CFC) family of vertebrate signaling ligands that was first isolated in human and mouse teratocarcinoma cells [20]. Cripto has been well characterized to be key regulator of embryonic stem cells during development, initially detected prior to gastrulation in the 4-day blastocyst and is needed for the formation of the primitive streak patterning of the anterior/posterior axis, specification of mesoderm and endoderm during gastrulation, and establishment of left/right (L/R) asymmetry of developing organs [21]. A well-known marker of embryonic and adult stem cells, Cripto is re-expressed in several malignancies in the adult to regulate cancer stem cells within mammary and melanoma carcinomas, among other cancer types [22,23]. Cripto functions via two distinct signaling mechanisms that involve pathways associated with stem cell behavior and tumorigenesis. It can function as a coreceptor of TGF-β ligands, Nodal and

Activin, to modulate Smad2/3 signaling activity [24,25,26]. In its soluble state detached from the cell membrane, Cripto activates SRC/MAPK/PI3K pathways independent of TGF-β, yet both signaling pathways require the mandatory binding of Cripto to heat shock protein, GRP78, at the cell surface in order for Cripto to function [27,28].

Although well implicated in stem cell maintenance and pluripotency, little research has been done on the role of Cripto in regeneration and wound healing. To understand the mechanisms in which Cripto may be aiding regeneration, we sought to discover novel Cripto binding partners. Through mass spectrometric and proteomic analysis, we identified the non-muscle myosin class II (NMII) proteins, MYH9 and MYH10, to be of the top five Cripto binding partners. Non-muscle motor proteins that interact with the actin cytoskeleton act as master regulators of cell morphology, NMII also play an important role in regeneration and stem cell activity. Although the expression of MYH9 remains relatively constant before and during neurite growth, the mRNA levels of MYH10 significantly increase during neurite outgrowth [29]. It has also been reported that inhibition of NMII upstream kinase, ROCK, induces neural differentiation of placental-derived multipotent cells [30].

Previous reports have shown that membrane proteins, including GPI-anchored proteins, can function in a paracrine manner through intercellular crosstalk by exosomal vesicles or direct cell-to-cell contact [31-33]. Our proteomic analysis of GRP78-MyosinII binders revealed that Rab11A, an intracellular vesicle trafficking marker, is a common co-binder. Rab11A has been shown to regulate the formation of transport vesicles and their fusion with the membrane and also control endocytic recycling [34,35]. Thus, we

hypothesize that the Myosin IIs and Rab11A may be regulating the localization and secretion of Cripto through an endocytotic and exosomal mechanism.

In our study, we report that blockage of Myosin II's decreases the levels of soluble and also membrane-bound Cripto. Also, inhibition of Myosin II's alters the localization of Rab11A and induces more intracellular co-localization of Cripto and Rab11A. *In vivo*, inhibition of Cripto and/or Myosin II also decreases regeneration and the addition of exogenous Cripto induces this process. This Cripto-dependent induction of regeneration can then be blocked by a Cripto inhibitor. Based on our findings, we propose a new model whereby MYH9/10-mediated Cripto transport enables cells to generate a pool of extracellular Cripto that can subsequently function in autocrine and/or paracrine pathways to promote stem cell mediated regeneration and wound healing.

Chapter 2: Materials and Methods

Zebrafish Husbandry

AB strain zebrafish were kept in secure vivarium module (Aquaneering, Inc., San Diego, CA) that was kept at 28°C on a 14 hours light and 10 hour dark cycle. Fish were fed twice a day on an original 1:1:1 ratio of Tetramin (Tetra, Blacksburg, VA), blood worms (Hikari, Hayworth, CA), and Goldfish Aquarium Fish Food Brand (O.S.I. Marine Lab, Burlingame, CA) three times a week. Twice a day, zebrafish were also fed brine shrimp (BioMarine, Hawthorne, CA). On weekends, zebrafish were not fed. Matings were set-up in the evenings at a 4 male to 3 female ratio. Baffles were removed at 8am the next morning and eggs were collected 2pm that day into petri dishes filled with E3 media (5mM NaCl, 0.17mM KCl, 0.33mM CaCl2, 0.33mM MgSO4, 10-5 % Methylene Blue). Eggs were then incubated at 28°C for five days and were then utilized for experimentation or transferred to the vivarium module.

Adult Zebrafish Amputations

For the adult, working area and utensils were first sterilized with RNAse Away (Molecular BioProducts, Inc., San Diego, CA). Zebrafish were put into a 0.02% solution (0.01 g) of the fish anesthetic, Tricaine (Western, Chemical, Inc., Ferndale, WA), in 50 mL of aquatic system water and were anesthetized within a period of no more than three minutes. Zebrafish were then placed underneath a stereoscope (AO Spencer Stereo Microscope) at 20X magnification and the caudal fin was then amputated using a surgical dissection blade. The regrowth tissue was also collected at the indicated time points after the initial amputation (4 per time point) and was placed inside 200μl of lysis buffer included in RNeasy Mini Kit (Qiagen, Netherlands). Samples were put on top of dry ice for further downstream applications or stored at -20°C.

Adult Zebrafish RNA harvest

RNA harvest took place inside standard chemical fume hood. Before beginning any RNA work, fume hood as well as working instruments were thoroughly cleaned with RNAse Away. Samples were then microhomogenized (Claremont BioSolutions, Upland, CA) for

a minimum of three minutes; a new microhomogenizer was used for each 9 sample. An additional 100 μl of lysis buffer from RNeasy Mini Kit was added to initial 200 μl and sample was further homogenized (Qiagen, Netherlands). Protocol provided from Qiagen was directly followed and gather product was quantified using Nanodrop 2000c Spectrophotometer (Thermo Scientific, Grand Island, NY) under nucleic acid setting and RNA option. RNA samples were stored at -20°C until use in cDNA synthesis (reverse transcriptase PCR).

Adult Zebrafish cDNA synthesis

Synthesis of cDNA was performed after all required samples were collected using the Maxima Universal First Strand Kit (Thermo Scientific, Grand Island, NY). All samples were processed at the same time for every round of caudal fin amputations using instructions included within the kit. cDNA products were quantified using Nanodrop 2000c Spectrophotometer (Thermo Scientific, Grand Island, NY).

Adult Zebrafish qPCR

Quantitative PCR (qPCR) was performed by using Maxima SYBR Green/ROX qPCR Master Mix using a 7300 Fast Real-Time PCR System (Applied Biosystems, Waltham, MA). All samples were run in triplicates for each primer (oep and hspa5). Zebrafish housekeeping gene used was rpl13a and it was also run in triplicates. Ct values were analyzed using Excel software and graphs were generated using Prism 6 software.

Zebrafish Fry Amputations

Amputations were performed on AB strain zebrafish frys at 5 dps. Frys were anesthetized in a 0.005% solution of Tricaine diluted in E3 media for no longer than 3 minutes. The caudal fin was then amputated using a surgical blade underneath a stereoscope at 20X magnification. Frys were then transferred into a petri dish of fresh E3 media to recover. Once recovered, frys were placed in 1mL of E3 media in a 24-well plate at 1 fry per well. The 0 hour time point of amputation was then imaged at 80X magnification (SteREO Lumar.V12, Carl Zeiss, Jena, Germany) and then treated with indicated treatments. 48 hours post amputation, the regrowth was then imaged again at 80X magnification.

Zebrafish Fry Quantification

Using Fiji, the 48 hour regrowth was quantified by measuring with a line tool the amount of regrowth from the initial amputation site at the 0 hour time point. The regrowth from viable frys were then averaged and divided by 2 to determine the amount of regrowth per 24 hours. Standard error means were also calculated.

Zebrafish Fry Treatments

ALK-4L75A-Fc (5 μg/mL) and IgG (5 μg/mL) was used as Cripto inhibitor and control. Blebbistatin (5 μg/mL) and DMSO was used as the Myosin II inhibitor and control. Frys were treated in 500uL/well in a 24-well plate per treatment. For soluble Cripto experiments, conditioned media was collected from 90-100% confluent MCF10A-Vector and –Cripto 10cm plates conditioned with 6mL of E3 media for 72 hours. The conditioned media was centrifuged at 1000rpm for 5 minutes and supernatant was then collected and applied to frys at 500uL/well.

Cell Lines

MCF10A and C3H10T1/2 cells were obtained from the American Tissue Culture Collection (ATCC) and were cultured as recommended by ATCC. MCF10A cells were cultured in DMEF12 growth media, supplemented with 5% horse serum, 10µg/mL insulin, 20ng/mL EGF, 0.5µg/mL hydrocortisone, 100ng/mL cholera toxin and antibiotics. C3H10T1/2 cells were cultured in DMEM/High-Glucose growth media supplemented with 10% FBS.

Wound Healing

Cell lines were plated at a high density of 8E5 cells/mL (MCF10A) or 2E5 cells/mL (C3H10T1/2) onto plastic or indicated extracellular matrix protein in a 24-well plate. The next day, a p20 pippette tip was used to scratch on "X" across the confluent layer of cells. Media was then removed and replaced with indicated treatment. Eight points were chosen per well and imaged for 24 hours Leica time-lapsed imaging. Fiji was then used to measure the distance of closure and Excel to calculate the rate of closure over time.

Random 2-D Migration

Cell lines were plated at 1E4 cells/mL in a 24-well plate either on plastic or indicated extracellular matrix protein. The next day, media was removed and replaced with Myosin II inhibitor, blebbistatin, treatment at 5,10, or 20uM concentration. Three points per well were chosen and then monitored over 24 hours through time-lapsed imaging. Fiji was then used to track cell displacement and velocity.

Western Blots

Conditioned media and cell lysates were collected for Western blot assay. Cells were grown to 90-100% confluency, and then treated with 5uM or 10uM blebbistatin. Approximately 24 hours later, cells were re-treated and conditioned in 6mL of 5uM or 10uM blebbistatin for 72 hours. Conditioned media was collected, cleared by centrifugation and protein concentration was determined via a Bradford Assay. Cells were lysed with Stringent RIPA Lysis Buffer and rotated at 4°C for 3 hours. Lysates were then cleared by centrifugation, and the protein concentration was determined via a Bradford Assay. Then 4–12% Bis-Tris gels were ran and transferred to nitrocellulose membranes. The membranes were then probed at 4C overnight with indicated antibodies with the following dilutions: Anti-Flag (Salk Institute 1:400), Cripto (Salk Institute 1:400), α-tubulin (cell signaling 1:1000), and GRP78 (Salk Institute 1:1000). Secondary antibodies were used at a 1:2,000 or 1:5,000 dilution.

Measurement of cell surface expression of Cripto

MCF10A derivatives and C3H10T1/2 cells were plated at a density of 100,000 and 20,000 cells per well in a 24-well plate. Media was removed the next day and cells were treated with 1mL of either 5uM or 10uM blebbistatin or DMSO as control. Approximately 24 hours later, cells were re-treated with the same prior treatment for 72 hours. An intact cell ELISA was then performed in which cells were fixed with 500uL of 4% paraformaldehyde diluted in PBS for 30 minutes at 4°C, washed with 500uL PBS for 15 minutes at 4°C, and then blocked with 3% Bovine Serum Albumin (BSA) diluted In PBS for 30 minutes at room temperature. MCF10A cells were then incubated for 1.5 hours with 250uL of 2ug/mL anti-FLAG antibody and C3H10T1/2 with 2ug/mL anti-

Cripto 6900 antibody in 3% BSA. For control wells, primary antibodies were not administered. Cells were then washed 3X with PBS at room temperature and then incubated with peroxidase-conjugated anti-rabbit secondary antibody at a 1:400 dilution for 1 hour at room temperature in 250uL. Cells were washed again 3X with PBS at room temperature and then treated with 250uL of TMB peroxidase substrate at room temperature until a blue color was visible. Reactions were stopped by adding 200 μL of 0.18M H_2SO_4 to each well, and peroxidase activity was quantified by measuring the absorbance of the resulting yellow solutions at 450 nm.

Live Cell Imaging

C3H10T1/2 cells were plated at a density of 34,500 cells in a single well of a 24-well plate. The next day, the cells were transfected with GFP-MYH9 plasmid via GenJet transfection agent. 24 hours later, the cells were transferred to a fibronectin-coated glass bottom culture dish (MatTek) and then imaged via fluorescent and phase-contrast microscopy using a Leica widefield-brightfield phase contrast microscope. The data was analyzed with Fiji (Image J) software. Student t-test analysis was performed to determine statistical significance.

Immunofluorescence/ Confocal Imaging

As described in the live cell imaging, C3H10T1/2 cells were plated and the next day treated with a various construct via FuGENE transfection agent. The next day, cells were plated onto a collagen-coated slide in a 6-well plate. The following day, the cells were treated for 8.5 hours in the various conditions and then an immunofluorescence was performed to tag endogenous Cripto and Myosin IIs at 1:500 dilution for primaries and 1:1000 dilution for secondaries. The slides were then imaged using the Leica TCS SP5 II confocal microscope at 20- and 100x magnification. Images were captured at 2048x2048 resolution at 10 frame average . The pinhole was set to 150um.

Cell Lysates and Co-immunoprecipitation

Cell lysates were prepared in radioimmunoprecipitation assay (RIPA) buffer as previously described [25]. For immunoprecipitation experiments, 1 to 5 mg protein extract was precleared by protein G-PLUS-agarose beads for 2 h at 4°C. The precleared extracts were incubated as indicated with 40 µl anti-FLAG M2 gel beads or 20 µl G-PLUS-agarose preincubated with 15 µl anti-MYH9 (KDEL), 10 µl anti-HA, or 25 µl anti-His for 2 h at 4°C. Immunoprecipitates were subsequently washed four times with RIPA buffer and two times with 54K buffer (50 mM Tris, pH 7.9, 150 mM NaCl, 0.5% Triton X-100). We then eluted the proteins either by heating the beads at 95°C in sample buffer or by adding 50 µl of Flag peptide (1 µg/µl), followed by the removal of any remaining associated proteins by heating in sample buffer.

Mass Spectrometric Analysis

Mass-specific bands were excised from a Coomassie blue-stained gel. Gel slices were further destained by treatment with 40% aqueous n-propanol and 50% aqueous acetonitrile. To the destained gel slice, 100 ng trypsin was added in 10 µl ammonium bicarbonate solution (20 mM). Digestion was allowed to proceed at 37°C for 16 h. One microliter of the supernatant was spotted onto a matrix-assisted laser desorption ionization target and mixed with 1 µl of a saturated solution of alpha-cyano-hydroxycinnamic acid. After being dried, the sample was analyzed on a Bruker Ultraflex TOF/TOF (Bruker Daltonics, Billerica, MA) instrument in positive reflected time-of-flight (TOF) mode. Mass fingerprint data were analyzed using the Mascot algorithm (Matrix Science, London, United Kingdom).

Exosome Enrichment

Exosomes were isolated and collected as previously described [36]. The conditioned media were collected and centrifuged for 15 min at 2380×g, and then further ultracentrifuged for 70 min at 110 000×g (Optima TL ultracentrifuge, Beckman Coulter, USA). The supernatants were collected, and were concentrated using Amicon Ultra-2 centrifugal filters (Millipore, USA) as exosome-depleted conditioned media (MSC-CM (exo−)). To isolate the exosomes (MSC-exosomes), the pellets were washed in

Phosphate-buffered saline (PBS) and a second ultracentrifugation was performed for 70 min at 110 000×g. The exosomes isolated from the same volumes of culture medium from the same numbers of cells were resuspended in PBS or DMEM for use as fresh preparation.

Bioinformatics Methods of Cripto Binders and Exosome Enrichment

After mass spectrometry was performed on cell lysates and exosomes from MCF10A-Vector and MCF10A-Cripto lines, our database of Cripto binders and exosomal proteins were analyzed with DAVID proteomics software for Gene Ontology analysis of cellular components and biological processes. The minimum fold change was cut off at 2.

Cell Cycle Analysis

C3H10T1/2 cells were plated at ___ and 2 mLs/well in a 6 well plate. The next day, 72hr conditioned media from MCF10A-Vector and –Cripto lines was added. 72hrs post treatment, cell cycle analysis was preformed. Cells were suspended in 1 mL of PBS and collected in a 15-mL conical tube. After addition of 2.5mL absolute ethanol (200 proof) to each sample, samples were incubated on ice for 15 minutes. After permeabilization of cell membranes via ethanol incubation, cells were centrifuged at 1500 rpm for 5 minutes and resuspended in PI solution (475uL of PBS, 25uL of 1mg/mL Propidium Iodide, 5 uL of 10mg/mL RNase A, and 0.25uL of 0.05% Triton X-100). Stained samples were incubated at 37 degrees Celsius for 40 minutes. After incubation, they were resuspended with 500 uL of PBS. We used the FL-2 channel (546nm) on a BD Facs Calibur instrument to characterize the samples' cell cycle profile.

Aqueous One

C3H10T1/2 cells were plated on plastic in complete media in a 96-well plate at 1E4 cells/mL and 200uL/well in triplicate. The next day, recombinant human Cripto (R&D Systems) at indicated concentrations or Cripto derived from conditioned media of the MCF10A-Vector or –Cripto cells, was applied to the cells, and then at indicated time points, 40uL of AQueous One reagent (Promega) was added to each wells and the wavelength was read at 490nm 1.5, 2 and 3 hours post-treatment.

Chapter 3: Results

Temporal expression of Cripto (oep) during zebrafish caudal fin regeneration correlates with adult stem cell genes.

Previous data has established Cripto as a regulator of embryonic and induced pluripotent stem cells. We first wanted to test if the temporal expression of the zebrafish Cripto homolog, one-eyed pinhead (oep), correlates with known progenitor stem cell markers in the adult zebrafish during caudal fin regeneration. The zebrafish caudal fin system of regeneration is a model that has been well-characterized and several markers of progenitor stem cells have been identified [37-41]. As positive controls, the expression pattern of progenitor markers for the blastema (msxb), scleroblasts (ptc1), and osteoblasts (sp7) were evaluated through qPCR at 0, 48, 96 and 192 hours post amputation (hpa). The temporal expression pattern of the stem cell markers is consistent in which the highest expression is shown at the 96 hpa time point **(Figure 1A).** This time point correlates with the formation of the blastema, a transient structure notably enriched for multipotent stem cells and critical for regeneration [14]. Next, negative markers of differentiated cell types, including endothelium (fli1a) and melanocytes (tryp1b) were tested for their temporal expression, yet expression pattern did not correlate with the progenitor stem cell markers. Although fli1a also peaks at 96 hpa, the expression slightly decreases at 192 hpa, in contrast to the stem cell markers by which the decrease is more drastic. Lastly, when testing the temporal expression of oep during the caudal fin regeneration, the pattern correlated with the stem cell markers. This finding may indicate a possible function for oep in these cell populations during tissue regeneration.

In order to test if the expression pattern of the selected positive and negative stem cell markers also correlate in mammals, we extrapolated RNA-seq data from Meyer et. al. JBC study. In their RNA-seq analysis, mouse bone derived mesenchymal stem cells were treated either with normal mesenchymal stem cell media (MSC) or bone differentiating media (MSC-Bone). Their data shows that the gene expression of Cripto, and the mouse homologues of msxb (MSX3) and ptc1 (PTCH1) decrease in the differentiated cell type **(Figure 1B)**. The osteoblast marker, sp7, increased in the bone differentiated cell type unsurprisingly because it is a critical regulator of osteogenesis. As mentioned before, the blastemal formation of zebrafish regeneration marks an important timepoint in stem cell activity, so we collected and cultured the *ex vivo* 96 hpa regrowth tissue from the adult zebrafish. Unfortunately, we were unable to repeatedly generate a large culture of the explants, but were able to capture a few time-lapsed movies of the *ex vivo* cultures **(Figure 1C).**

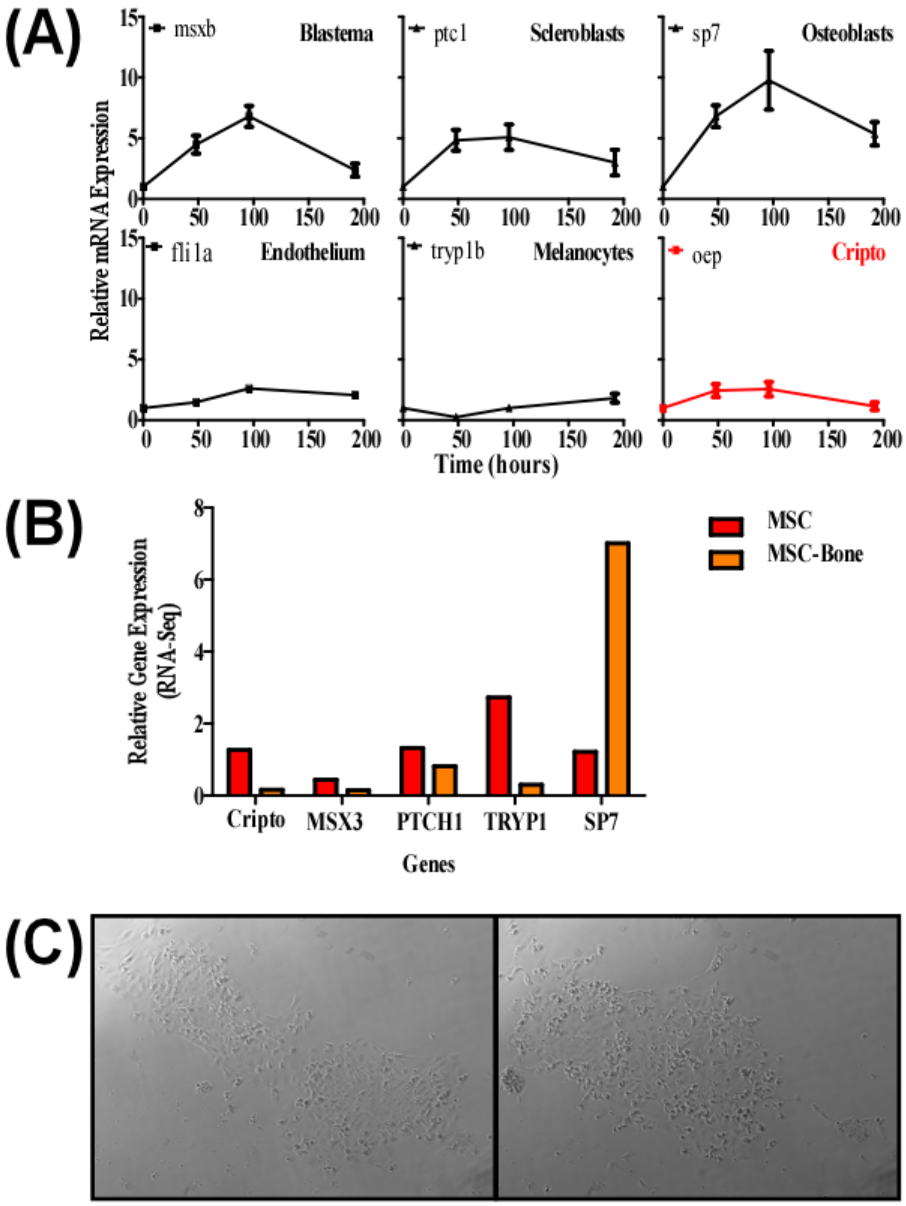

Figure 1. **(A)** qPCR analysis of progenitor (stem) and differentiated cell markers as well as Cripto expression. RNA was obtained at the indicated time points following amputation of the caudal fin in the adult zebrafish. **(B)** RNA-seq data of progenitor, differentiated markers as well as Cripto gene expression in mesenchymal stem cells (MSC) treated with normal or bone differentiating (MSC-bone) media. Analysis extracted from Meyer et al., JBC (2016). **(C)** *Ex vivo* culture of adult zebrafish regrowth tissue collected at 96 hours after amputation (hpa).

Inhibition of Cripto blocks Zebrafish tail regeneration.

Next, we wanted to test the functional role of Cripto (oep) during regeneration by using a Cripto inhibitor and the juvenile zebrafish tail bud regeneration model since this assay is amenable to pharmacology studies. The Cripto inhibitor, LF5A-Fc, had been engineered using a soluble human Fc chimera of the ALK4 receptor extracellular domain containing a point mutation at L75 (L75A-Fc). Previous studies had shown that the Cripto antagonist was capable of inhibiting growth-factor-like effects of soluble Cripto in mammary epithelial cells, but had never been used in the zebrafish [42]. Because the Cripto inhibitor was developed in humans, we aligned the human, mouse, and fish Cripto amino acid sequence to ensure that necessary L75A-Fc binding sites regions were conserved for Cripto inhibition in the juvenile tail bud assay (**Figure 2B**). By performing the experimental procedure detailed in **Figure 2A**, our data reveals that inhibition of Cripto significantly blocks juvenile zebrafish regeneration by nearly 50%, decreasing from approximately 40 um to 20 um per day (**Figure 2D**). This effect is also visualized in the micrographs taken 48 hpa and post-treatment (**Figure 2C**). Next, by adding soluble Cripto to the regenerating juvenile tail bud, regrowth was enhanced and this effect could also be blocked by the Cripto inhibitor (**Figure 2C**). Collectively, these results show a Cripto dependent response in zebrafish tail bud regeneration.

Using the MSC line, C3H10T1/2, we tested the effect of recombinant human Cripto on cell proliferation/survival *in vitro* and saw that the addition of Cripto induced this phenotype. We then further analyzed the effect of soluble Cripto in conditioned media collected MCF10A-Vector and Cripto lines. Adding soluble Cripto to the MSC altered the cell cycle profile by shifting the G0/G1 phase to the synthesis (S) phase

compared to the vehicle (**Figure 2D**). This data suggests Cripto may be promoting proliferation in MSC to increase regeneration.

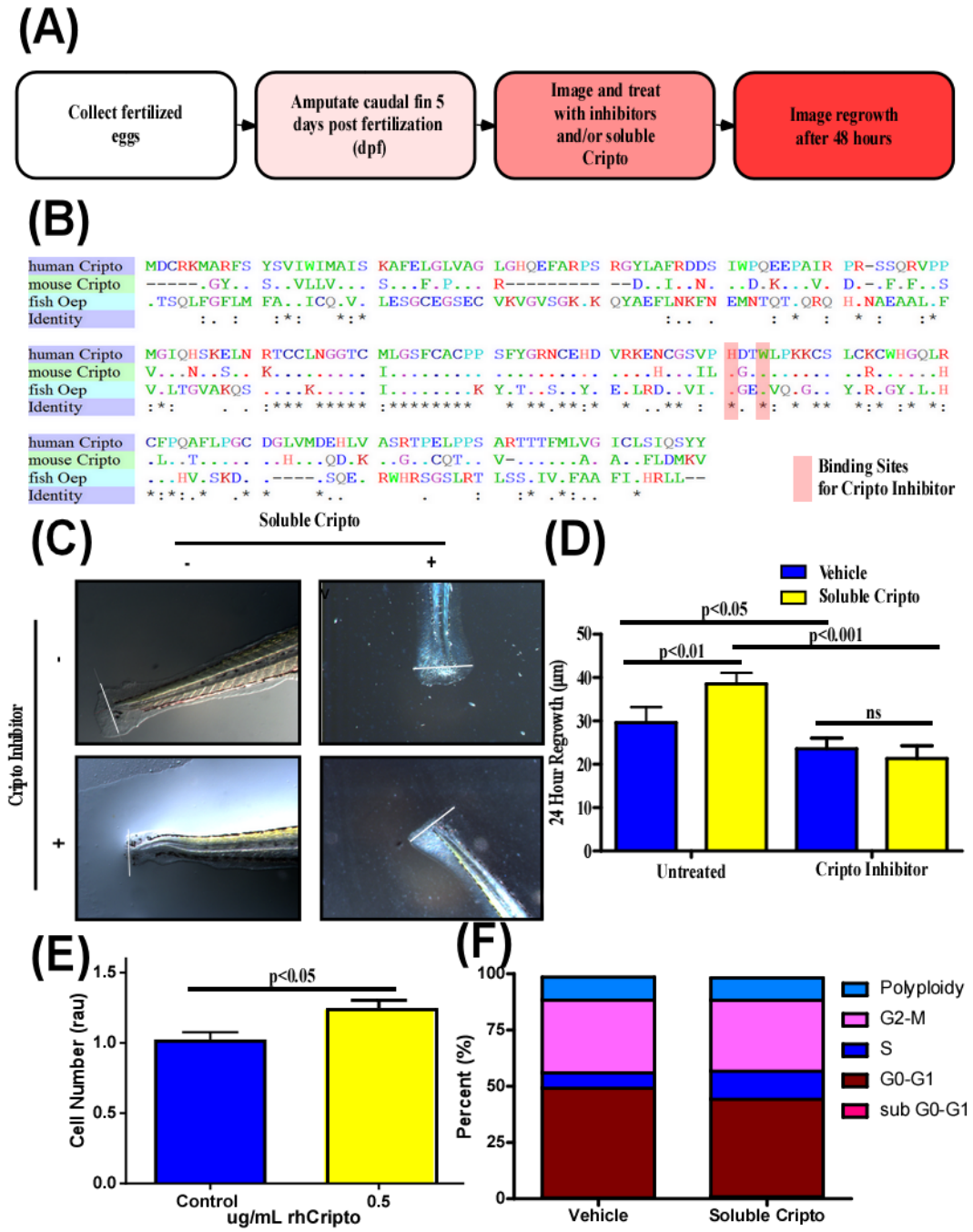

Figure 2. **(A)** Schematic of method for quantifying caudal fin regrowth in the juvenile zebrafish fry system. **(B)** Protein sequence alignment of human, mouse and fish Cripto (oep). Shaded pink regions represent the mandatory Cripto inhibitor binding sites that are conserved in all three species. **(C)** Images of the control and Cripto inhibitor treated tails with vehicle or soluble Cripto at 48 hours post amputation (hpa). **(D)** The 24 hour mean regrowth (µm) of tails treated with vehicle or soluble Cripto in the absence and presence of Cripto inhibitor. The mean regrowth was calculated by measuring the length of regrowth after 48 hpa using Fiji software and then divided by 2 to calculate the mean regrowth per 24 hours. (F) Cell proliferation/survival of MSCs treated with recombinant human Cripto was measured using AQueous One assay. **(E)** Cell cycle analysis of mesenchymal stem cell line, C3H10T1/2, treated with vehicle or soluble Cripto.

Myosin IIs are Novel Cripto Binders that Function in Overlapping Pathways with Cripto to Mediate Zebrafish Caudal Fin Regeneration.

To elucidate potential mechanisms by which Cripto may be regulating stem cell-mediated tissue regeneration, we sought to identify novel Cripto binding proteins. Described in the experimental flowchart in **Figure 3A**, our collaborators at the Salk Institute collected total cell lysates and performed a Flag-Cripto IP from Empty Vector- or Flag-tagged Cripto-overexpressing mammary epithelial cells, MCF10A. MudPIT mass spectrometry analysis revealed a total of 59 proteins that had at least a 2-fold increase in peptide count comparing MCF10A-Vector versus Cripto cell lines. We then used DAVID proteomics to analyze the gene ontologies, including biological processes and cellular components, our list of Cripto binders were enriched for (**Figure 3B and 3C**). Notably, the Myosin II proteins were of the top five binders, as well as GRP78, a heat shock protein previously discovered to be an essential upstream regulator of Cripto activity.

To validate the binding association of Cripto and Myosin IIs, a co-immunoprecipitation assay was performed using the MCF10A-Vector and -Cripto lines, and then immunoprecipitated for the Myosin II, MYH9 (**Figure 3D**). Co-localization of endogenous MYH9 (Green) and Cripto (Red) was also visualized in the mesenchymal stem cell line, C3H10T1/2, to further validate Myosin IIs as novel Cripto binding proteins (**Figure 3E**). We next wanted to investigate the role of Myosin II's during zebrafish caudal fin regeneration. In the same system in which Cripto was blocked in the zebrafish frys, Myosin II's were next blocked and resulted in a significant decrease of regrowth tissue compared to the control treatment (**Figure 3F** and **G**). In a dual inhibition

experiment in which the frys were treated with both the Cripto and Myosin II inhibitors simultaneously, there is no additive or synergistic effect, suggesting that the proteins may be working in an overlapping pathway to mediate this process (**Figure 3F** and **3G**).

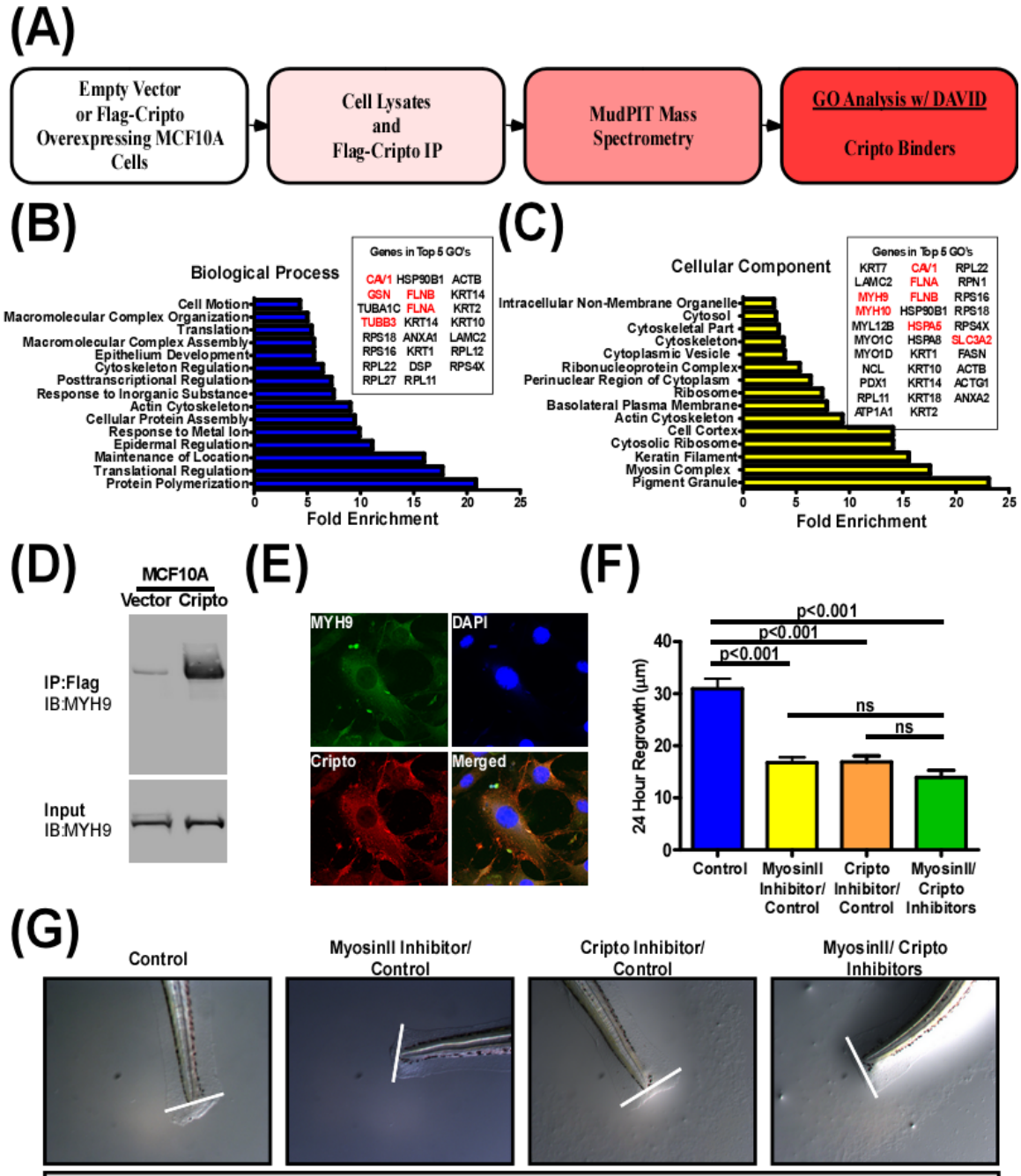

Figure 3. **(A)** Schematic of method for identifying novel Cripto binders. **(B and C)** Biological processes and cellular components of Cripto binders. Genes highlighted in red the top Cripto binders. **(D)** Cripto (Flag-tagged) co-immunoprecipitation and total lysates samples immunoblotted for Myosin IIA (i.e., MYH9). **(E)** Confocal imaging of endogenous Myosin IIA (i.e., MYH9) (Green) and Cripto (Red) protein expression and colocalization shown in mesenchymal stem cell line, C3HT101/2. **(F)** The 24 hour mean regrowth (um) of tails treated as indicated. **(G)** Images of the 48 hpa caudal fin regrowth treated in **(F)**. p-values were calculated using a Student's t-test.

Myosin IIs Function to Promote Soluble and Intact Cell Surface Levels of Cripto.

As mentioned before, Cripto serves as a GPI-anchored protein that can be cleaved off as a soluble factor [26,43-44]. Myosin II's have been shown to play a role in protein trafficking via the Golgi network, so we hypothesized that the myosin II's may be involved in the localization of Cripto to the cell surface [45]. To test this hypothesis, total cell lysates and conditioned media were collected from MCF10A-Vector and –Cripto lines that were treated with either a control or myosin II inhibitor (**Figure 4A**). Alpha-tubulin was used as the loading control for lysates, and since no loading control can be used for conditioned media, it is not detected in those samples.

Immunoblotting for heat shock protein, GRP78, was performed since it is known to not only bind but also regulate Cripto signaling [46]. Even protein expression is shown for GRP78 in the cell lysates of both MCF10A-Vector and –Cripto cells despite Myosin II inhibitor treatment. When blotting for Cripto, it was not shown to be detected via Western blot in the Vector cell line, however, it is evenly detected in MCF10A-Cripto cell lysates in both control and Myosin II inhibitor treatments. Strikingly, soluble is Cripto is nearly blocked in the conditioned media when treated with the Myosin II inhibitor. The same experiment was then conducted in the C3H10T/12 cells at additional time points (**Figure 4B**). GRP78 is evenly detected in the cell lysates and also expressed at the 96 hour time point in the conditioned media. Cripto is also detected evenly in the cell lysates and only at the 96-hour time point in the conditioned media. An intact cell surface ELISA was then conducted to detect the levels of Cripto tethered to the cell membrane (**Figures 4C & D**). In the MCF10A-Cripto and C3H10T/12 lines, inhibiting

myosin II's significantly decreases the levels of Cripto at the cell surface. Collectively, these data suggest that the Myosin II's are critical for the trafficking and secretion of Cripto at the cell surface but also gives evidence that the secretion of soluble Cripto is not dependent on its trafficking to the cell surface.

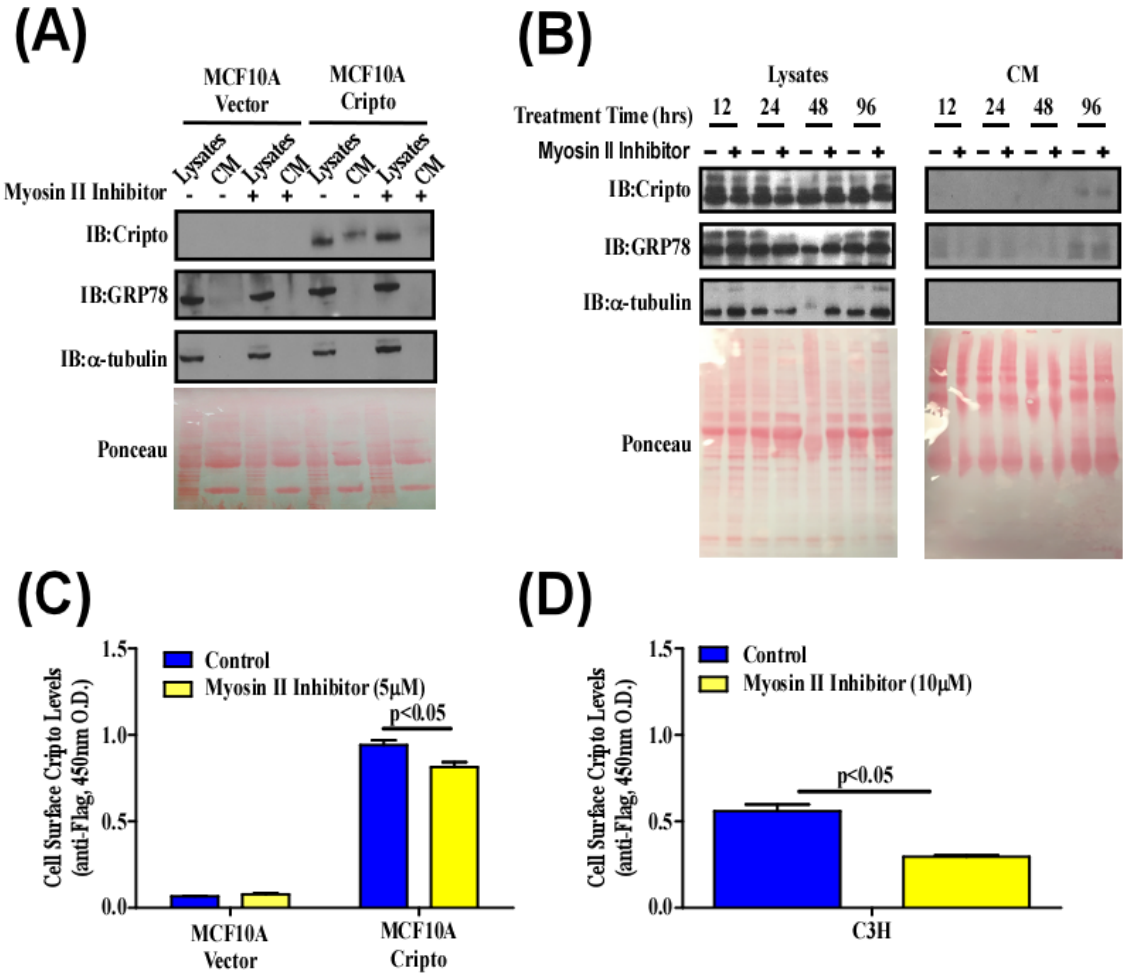

Figure 4. **(A and B)** Western blot and Ponceau Stain for indicated proteins in cell lysates and conditioned media (C.M.) from MCF10A-Vector and -Cripto lines **(A)** or C3H line **(B)** pre-treated and collected at indicated time points. **(C and D)** Intact ELISA quantification of cell surface Cripto levels after treated as indicated in MCF10A-Vector and -Cripto lines **(C)** or C3H line **(D)**. p-values were calculated using a Student's t-test.

ROCK or Myosin II Inhibition Increases the Psuedopodia/Cell Body Ratio and Co-localization of Cripto/MYH9 in MSCs.

Next, we wanted to test the effect of Myosin II inhibition on cell morphology and behavior. C3H10T/12 cells were plated on plastic and treated with DMSO, ROCK inhibitor, or Myosin II inhibitor in 0% FBS media. ROCK is a well-known upstream target of the Myosin IIs, and was used as an alternative treatment to block Myosin II activity. Interestingly, at the 8.5 hour time point, the cell morphology is most striking in the ROCK and Myosin II inhibited treatments (**Figure 5A**). The ratio of pseudopodia to cell body increases, and the cells generate long and spindled pseudopodia protrusions. Confocal imaging was then performed to visualize the localization of endogenous Cripto and MYH9 in the ROCK and Myosin II inhibited treatments (**Figure 5B**). Imaged at 100x magnification, our images show that inhibition of ROCK and Myosin IIs increases co-binding and peri-nuclear localization of Cripto and the Myosin IIs in mesenchymal stem cells.

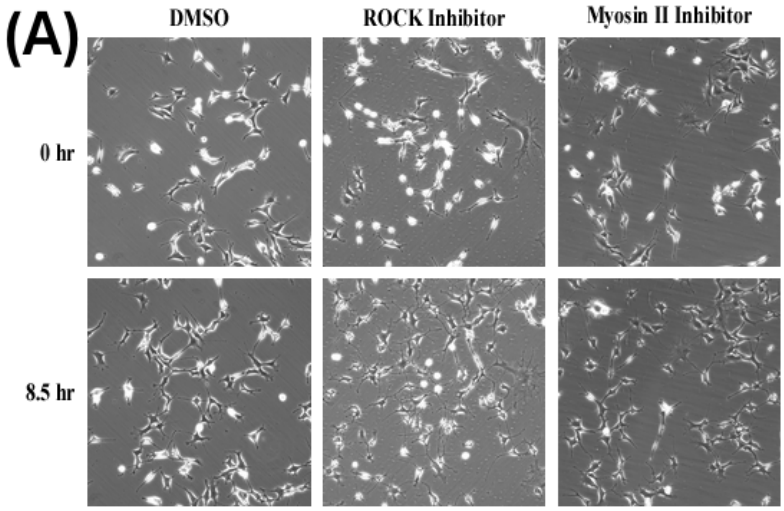

Figure 5. **(A)** Phase-contrast images taken at 0 and 8.5 hours of C3H cells treated with DMSO, ROCK inhibitor (Y26632, 10um) and Myosin II Inhibitor (Blebbistatin, 50uM). **(B)** Confocal imaging of endogenous Myosin IIA (i.e., MYH9) (Red) and Cripto (Red) protein expression and colocalization shown in mesenchymal stem cell line, C3HT101/2 treated as in (A) in 0% FBS media at 100x. Cripto (Green), MY9 (Red), and DAPI (Blue).

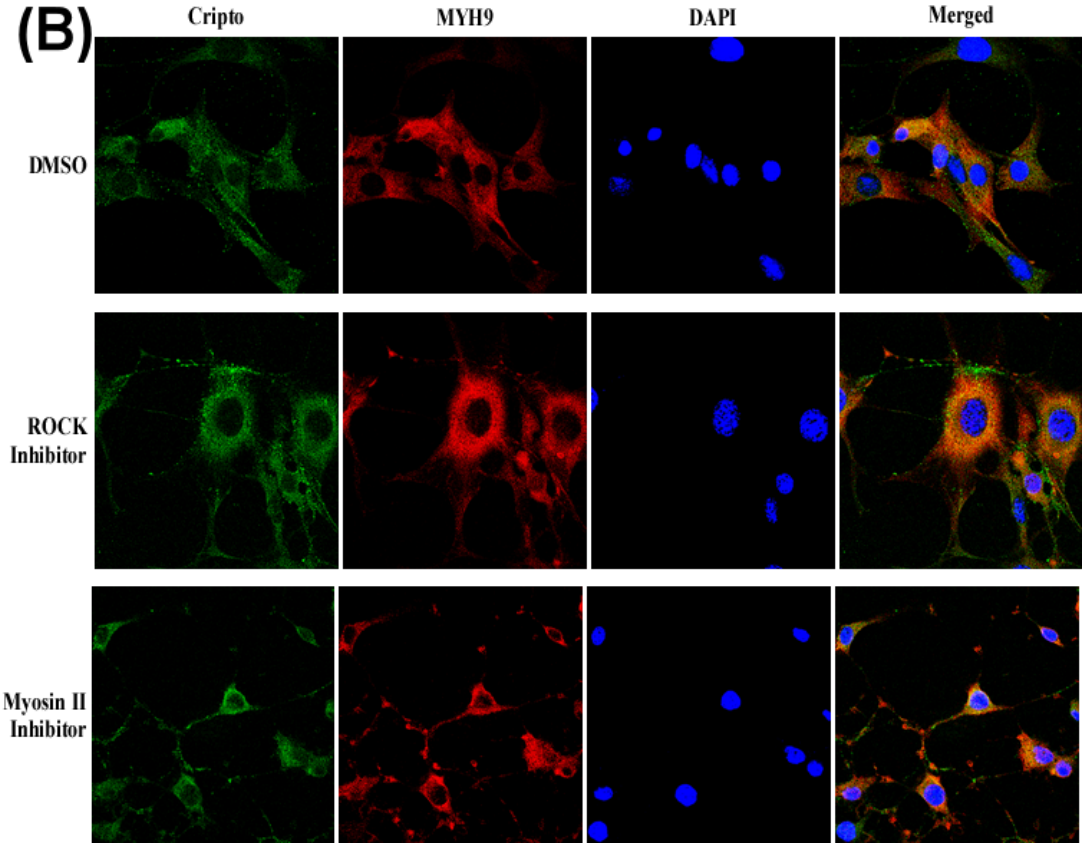

GO Analysis of Cripto/GRP78/MyosinII Binding Proteins and Cripto-Dependent Exosomal Proteins Suggest that Cripto Regulates Endocytosis and Extracellular Vesicle Contents.

Our data thus far has shown that the Myosin IIs are regulating the secretion of Cripto as an extracellular factor, yet the mechanism in which Cripto is being secreted is still unclear. Extracellular vesicles, referred to as exosomes, have been shown to be released by mesenchymal stem cells and contain pro-regenerative properties. We hypothesized that Cripto may be contained and, also regulating extracellular vesicle components. To test this, exosomes were collected from MCF10A-Vector -Cripto cell lines and their contents were then further analyzed through mass spectrometry (**Figure 6A)**. These proteins were then analyzed through DAVID proteins for their gene ontologies (**6B** and **6C**). Strikingly, we discovered that the MCF10A-Cripto exosomes had a distinct exosomal protein population than the MCF10A-Vector lines. We then used BioGrid to identify GRP78 and Myosin II co-binders, and performed DAVID proteomics for their gene ontologies (**Figure 6D and 6E**). Rab11A, a key regulator of intracellular membrane trafficking, was one of proteins from our list of co-binders. A Western blot was also performed in which we validated that Cripto is contained in exosomes (**Figure 6F**).

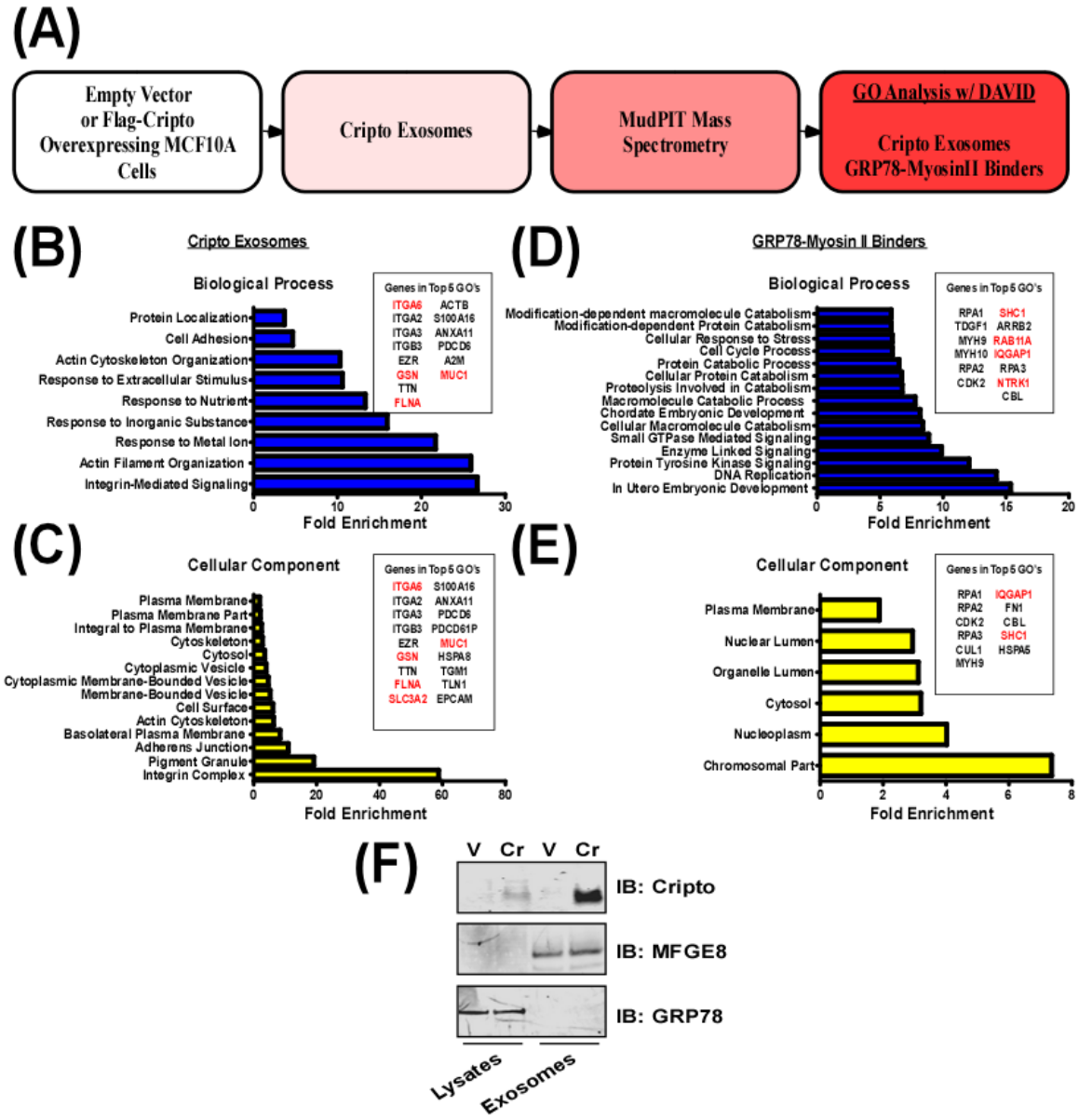

Figure 6. **(A)** Schematic of method for identifying Cripto Exosomes, and GRP78-Myosin II binder proteins. **(B-C)** Biological processes and cellular components of Cripto exosomes, and **(D-E)** GRP78-Myosin II binder proteins. **(F)** Western blot of lysates and exosomes from MCF10A-Vector and -Cripto cell lines.

Rab11A is a Potential Regulator of Myosin/Cripto Binding Interaction

We next explored the role of Rab11A in the binding interaction of Cripto and Myosin II by transfecting wildtype (WT), constitutively active (CA), and dominant negative (DN) Rab11A constructs into MSCs. Following transfection, the cells were then subjected to either Myosin II or ROCK inhibitors, or a control. We observed that overexpression of Rab11A in its CA form increased cell size and psueodopodial protrusions (**Figures 7, 8, & 9 d-f**) . This phenotype was also exhibited when Myosin II was inhibited, regardless of Rab11A expression (**Figures 7 & 9 b-c, e-f, and h-i,**). These data suggests an opposing role of Myosin II and Rabl11a in the regulation of MSC size and psuedopodial formation.

Next, we assessed the effect of Rab11A and Myosin II inhibition on the intracellular localization of Cripto, MYH9, and Rab11A. Here, we see that blocking Myosin IIs relocalizes Rab11A WT from cytoplasmic to perinuclear regions of the cell, however, Rab11A CA rescues this effect and relocalizes Rab11A back to the cytoplasm (**Figures 7 & 8 a-f**). The effect of Myosin II inhibition on MYH9 and Cripto relocalization to perinuclear sites is also rescued in the presence of Rab11A CA (**Figure 9a-f**). Additionally, Cripto and the Myosin IIs accumulated in psuedopodial regions of the Rabl1 CA MSCs, yet this phenotype is also displayed when Rablla DN is expressed, suggesting that this effect is not Rab11A dependent (**Figure 9**).

Lastly, we examined the potential role of Rab11A and Myosin IIs on the colocalization of Myosin IIs and Rab11A (**Figure 7**), Cripto and Rab11A (**Figure 8**), and Cripto and Myosin IIs (**Figure 9**). In Rablla WT, Cripto and MYH9 colocalization is shifted from cytoplasmic to perinuclear in the presence of Myosin II inhibitors (**Figure**

9a-c). In Rab11A CA, Myosin II inhibition induced Cripto and MYH9 co-localization to the pseudopodia versus the cytoplasm shown in the control (**Figure 9d-f**). Rab11a DN, however, decreases Cripto and MYH9 co-localization throughout the cell, but ROCK inhibitor treatment relocalizes their binding perinuclear (**Figure 9g-i**). ROCKi also promotes Rab11A and MYH9 co-binding despite Rab11A expression (**Figure 7c, f, and i**). Cripto and Rab11A interaction in the Rab11A WT is shifted from cytoplasmic to perinuclear upon Myosin II inhibition, yet their localization does not change when Rab11A is CA (F**igure 8a-f**). Rab11A DN changes Cripto-Rab11A co-localization from cytoplasmic/ perinuclear to the pseudopodia in response to Myosin II inhibition (**Figure 8g-i**). Thus, Rab11A serves as a novel regulator of Cripto and Myosin II binding activity and intracellular localization. These results are summarized in **Table 1**.

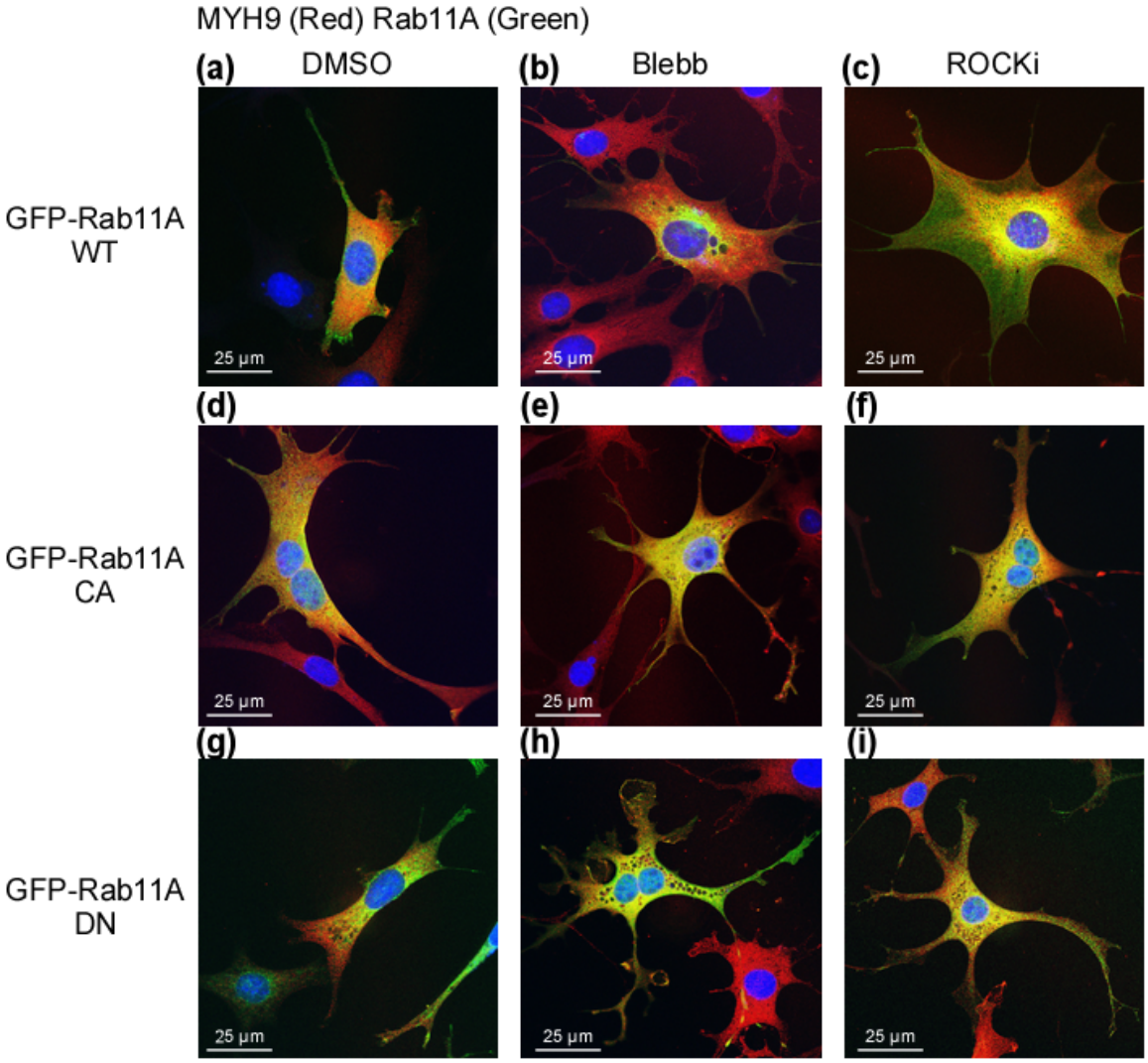

Figure 7. **(a-i)** Confocal images at 100x of C3H10T1/2 cells transfected with either wildtype (WT), constitutively active (CA) or dominant negative (DN) Rab11A and treated with control or Myosin II inhibitors, blebbistatin or ROCKi. Myosin II shown in red and Rab11A in green.

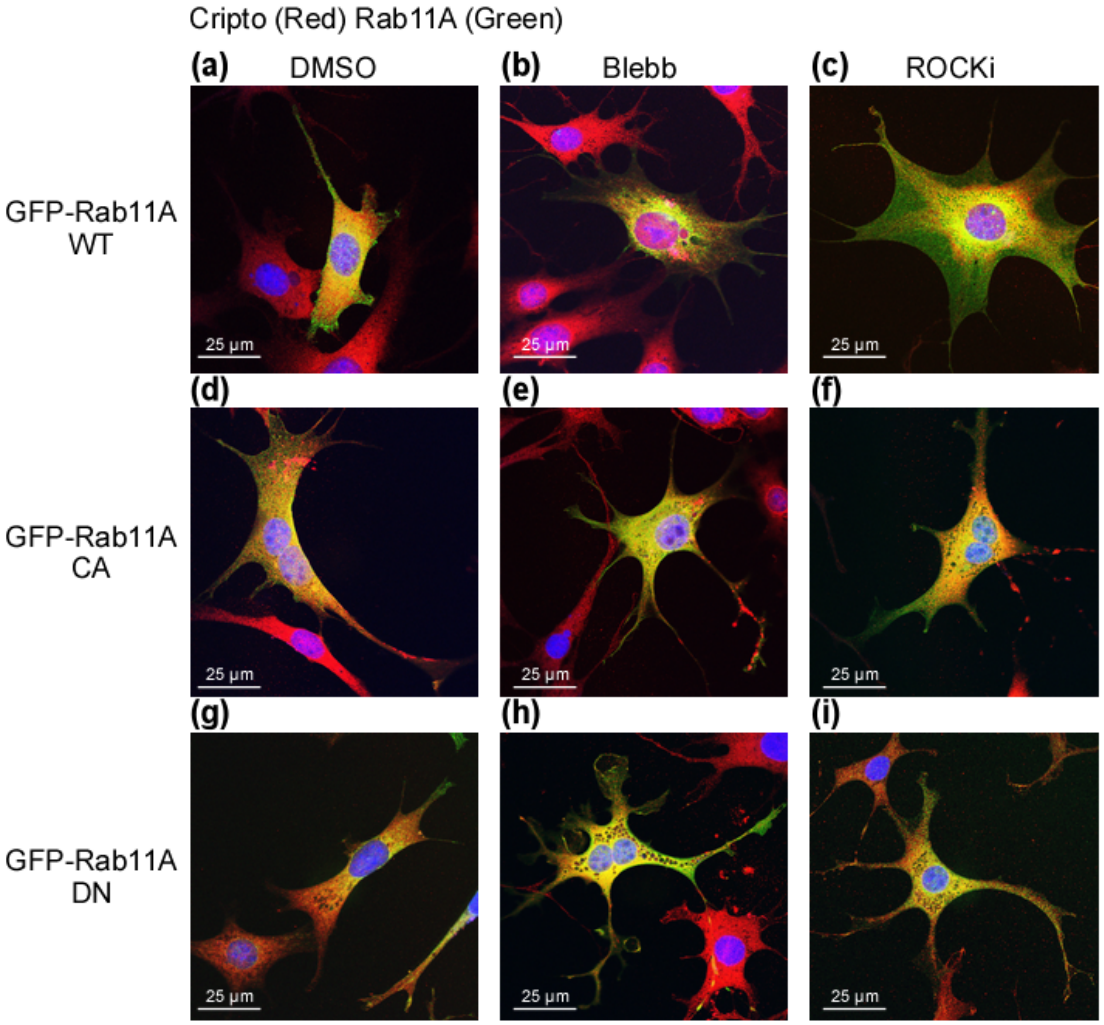

Figure 8. (**a-i**) Confocal images at 100x of C3H10T1/2 cells transfected with either wildtype (WT), constitutively active (CA) or dominant negative (DN) Rab11A and treated with control or Myosin II inhibitors, blebbistatin or ROCKi. Cripto shown in red and Rab11A in green.

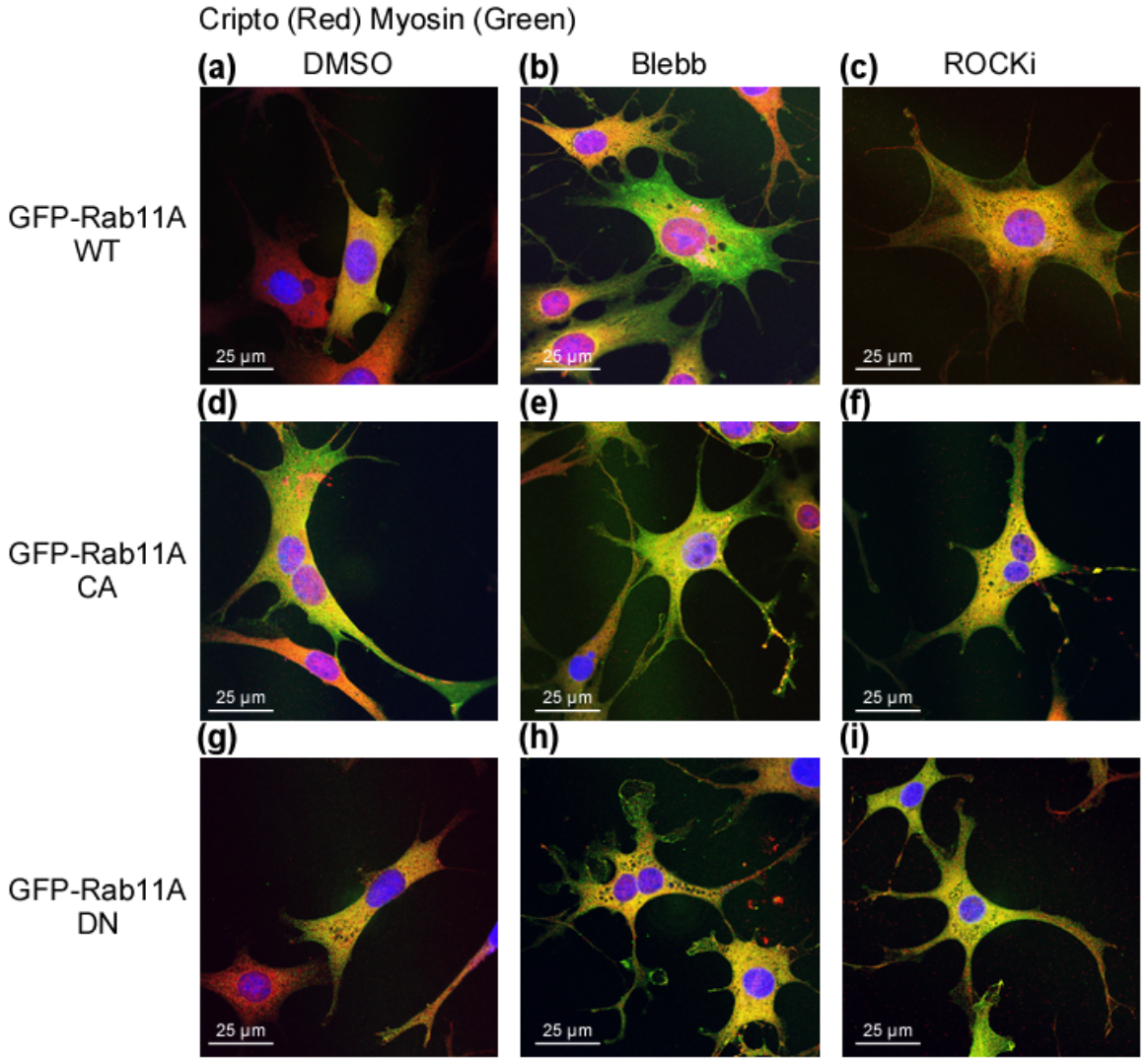

Figure 9. (**a-i**) Confocal images at 100x of C3H10T1/2 cells transfected with either wildtype (WT), constitutively active (CA) or dominant negative (DN) Rab11A and treated with control or Myosin II inhibitors, blebbistatin or ROCKi. Cripto shown in red and Myosin II in green.

	Properties & Proteins		DMSO	Blebb (10 uM)	ROCKi (10 uM)
Rab11A WT	Cell Size		(-)	(-/+)	(+)
	Protrusions		(-)	(+)	(-/+)
	Intracellular Localization	Rab11A	Cytoplasmic/Psuedopodial	Perinuuclear	Cytoplasmic/ Perinuclear
		Cripto	Cytoplasmic	Perinuclear	Perinuclear
		MYH9	Cytoplasmic	Cytoplasmic	Cytoplasmic/ Perinuclear
	Co-localization	M-R	(-/+) Cytoplasmic	(-)	(+) Perinuclear
		C-R	(+) Cytoplasmic	(+) Perinuclear	(+) Perinuclear
		M-C	(+) Cytoplasmic	(+) Perinuclear	(+) Perinuclear
Rab11A CA	Cell Size		(-/+)	(-/+)	(-/+)
	Protrusions		(-/+)	(+)	(+)
	Intracellular Localization	Rab11A	Cytoplasmic	Cytoplasmic	Cytoplasmic
		Cripto	Cytoplasmic/ Psuedopodial	Cytoplasmic/ Psuedopodial	Cytoplasmic/ Psuedopodial
		MYH9	Cytoplasmic	Cytoplasmic/ Psuedopodial	Cytoplasmic/ Psuedopodial
	Co-localization	M-R	(+) Cytoplasmic	(+) Cytoplasmic	(+) Cytoplasmic
		C-R	(+) Cytoplasmic	(+) Cytoplasmic	(+) Cytoplasmic
		M-C	(+) Cytoplasmic	(+) Cytoplasmic/ Psuedopodial	(+) Cytoplasmic/ Psuedopodial
Rab11A DN	Cell Size		(-)	(-/+)	(-/+)
	Protrusions		(-)	(+)	(+)
	Intracellular Localization	Rab11A	Cytoplasmic/ Perinuclear	Cytoplasmic/ Psuedopodial	Cytoplasmic/ Psuedopodial
		Cripto	Cytoplasmic	Cytoplasmic/ Psuedopodial	Cytoplasmic/ Psuedopodial
		MYH9	Cytoplasmic	Cytoplasmic/ Psuedopodial	Cytoplasmic
	Co-localization	M-R	(-)	(-/+) Pseudopodial	(+) Cytoplasmic
		C-R	(-/+) Cytoplasmic/ Perinuclear	(-/+) Cytoplasmic/ Psuedopodial	(-/+) Cytoplasmic/ Psuedopodial
		M-C	(-/+) Cytoplasmic	(-/+) Cytoplasmic	(-/+) Cytoplasmic/ Perinuclear

Table 1. Diagram table of Rab11a constructs and Myosin II inhibitor treatment effects on cell morphology and intracellular and co-localization. (-) indicates low levels, (-/+) intermediate, and (+) high. (M) MYH9, (C) Cripto, and (R) Rab11a.

Chapter 4: Discussion

At the cellular and molecular level, cells and tissues are constantly undergoing repair and regeneration in response to local stimuli, and require the self-renewing and pluripotent properties of adult stem cells to maintain proper wound healing events. In particular, multipotent mesenchymal stem cells have been shown advantageous in their therapeutic ability to treat degenerative diseases such as diabetes, stroke, and myocardial infarction [47-49]. MSCs display an exceptional regenerative capacity to treat tissue injury and immune disorders, yet the molecular factors that govern their behavior have yet to be fully elucidated in the field.

Here, we provide evidence that Cripto, a well-established gene signature of embryonic and induced pluripotent stem cells, is endogenously expressed in the MSC line, C3H10T1/2 [27,42]. Conditioned media (CM) collected from mammary epithelial cells (MCF10A) transduced with Cripto stimulated MSC proliferation in MSCs compared to the CM collected from an empty vector source. Cell cycle analysis showed that Cripto CM shifted the cell cycle from G0/G1 phase to the S, or synthesis phase, compared to the control. The addition of recombinant human Cripto also enhanced MSC proliferation and survival, suggesting a novel growth factor role of Cripto in MSCs.

A well-established member of the Epidermal Growth Factor-Cripto-1-FRL-1-Cryptic (EGF-CFC) family of proteins, Cripto serves as an obligate co-receptor for transforming growth factor beta (TGFβ) ligands, such as nodals, growth and differentiation factor 1 (GDF1), and GDF3 [24,25,50]. Cripto in its soluble form can act as a growth factor and was reported to enhance endothelial and mammary cell migration *in vitro* [42,51]. MSCs have also been reported to stimulate cell proliferation and

decrease apoptosis by producing various trophic factors, including vascular endothelial growth factor (VEGF), insulin-like growth factor 1 (IGF-1), basic fibroblast growth factors (bFGF), hepatocyte growth factor (HGF), IL-6 and CCL-2 [52-54]. Future studies can be generated to further investigate soluble Cripto's therapeutic capacity as a growth factor in MSCs.

Despite the advantageous benefits of MSCs, there are still major issues that challenge their widespread usage for injury repair. In contrast to iPS and ES cells, MSCs do not form teratomas or revoke any ethical concerns, and have a low immunogenicity [55,56]. MSCs are present in nearly all tissue types and can easily be isolated and expanded *in vitro* into mesoderm, ectoderm and endoderm tissue lineages [57-60]. Several studies have shown, however, long term culturing of MSCs can lead to an increase in histocompatibility complex (MHC II), and researchers continue to explore more effective methods of homing MSCs into host tissue [61,62].

We also provide novel data in Cripto's regenerative capabilities *in vivo* using the zebrafish caudal fin as our model system. Blockade of Cripto decreased the amount of tail bud regrowth by nearly 50% at 48hpa. In contrary, the addition of exogenous Cripto induced more growth versus the vehicle treated yet this effect was blocked in the presence of the Cripto inhibitor, suggesting a Cripto-dependent effect on tail bud regeneration. The non-muscle Myosin IIs also display the same phenotype when inhibited, and simultaneous treatment of both Cripto and Myosin II inhibitors did not elicit an additional response, suggesting a common pathway between Cripto and Myosin IIs in mediating caudal fin regeneration.

Proper patterning and deposition of blood is a critical component in the regrowth of caudal fin. Once blastema stem cells come into contact with the epidermal layer, they can differentiate into scheleroblasts, which then secrete dermal bone matrix [63]. The bone matrix progressively mineralizes to create new bony ray segments that are gradually added to the distal tip of the fin. Sonic hedgehog (shh), patched1 (ptc1), and bone morphogenic protein 2b (bmp2b), bmp4, and bmp6, are reported to be key regulators of skeletal deposition and patterning during caudal fin outgrowth [63,64-65]. Using a high-throughput surface plasmon resonance, a recent study revealed that soluble forms of Cripto inhibited BMP-4 signaling yet in accordance with other reports, membrane bound Cripto potentiated BMP-4 signaling [66]. Future studies can further investigate Cripto's role in BMP signaling in zebrafish and mammalian systems of regeneration.

We furthermore propose Myosin IIs to be novel Cripto binders that regulate the secretion of soluble Cripto. Inhibiting Myosin IIs blocked the production of Cripto in the CM collected from mammary epithelial cells transduced to overexpress Cripto. Surprisingly, C3H10T1/2 cells were able to secrete Cripto only at the 96 hour timepoint, yet their levels were unaffected by Myosin II inhibitor treatment. Blocking Myosin IIs also decreased the level of Cripto at the cell surface in MCF10A-Cripto and C3H10T1/2 lines. These results propose a novel mechanism governing Cripto secretion that has not been fully understood in the field.

Previous studies have shown that phospholipase C and D mediate membrane anchored Cripto cleavage, though recent and emerging evidence have suggested an endosomal recycling mechanisms of Cripto at the cell surface [51]. Blanchet et al reported Cripto as the first GPI anchored protein shown to control intraendosomal sorting

of its associated cargo, Nodal [67]. Cripto is able to stimulate Nodal activity by localizing Nodal at the endosome interface with intracellular effectors. Previous reports have also demonstrated that budding bulk endosomes in neurosecretory cells are surrounded by an acto-myosin II ring that promotes their fission from the plasma membrane [68]. It was also shown that Rho/ROCK and Myosin IIs regulate the polarized distribution of endocytic clathrins structures in the uropod of T lymphocytes [69].

We further suggest Rab11A to be a novel regulator of Cripto and Myosin II functionality in MSCs that may aid in the trafficking of soluble Cripto through exosomal and endosomal mediated pathways. Exosomes originate from early endosome bodies and can be a potential mechanism in which extracellular Cripto is secreted. Through data collected by BIOGRID protein interaction database, Rab11A was shown to be a Myosin II and GRP78 binder. Rab11A is a small GTPase that serve as key regulators of intracellular membrane trafficking. It is reported to function in the trafficking of recycling endosomes in polarized epithelial cells [70], also the docking and fusion of multivesicular bodies in leukemic cells [71]. A direct interaction of Rab11A and Myosin IIs in the promotion of recycling endosomes in Drosophilia was also reported, yet their interaction in the context of exosome production has not been studied in the field [72].

In our study, we show that Rab11A and Myosin IIs have opposing roles on cell size and protrusions. Studies have reported Myosin IIs inhibition to restrict cell size and shape in cell types such as the lung epithelial, but currently there are no studies that suggest a direct role of Rab11A in cell morphology [73]. We further show a cooperative role of Rab11A in Cripto and Myosin II binding and localization and future studies can be conducted to explore the role of Rab11A in wound healing and regenerative events.

In conclusion, we propose in our working model that Cripto is transported to the cell surface via Myosin IIs. Next, cell surface or membrane-bound Cripto can bind to the ALK4 receptor and TGF-beta ligands. Next, Cripto can be endocytosed into the cell via Rab11A vesicles. Myosin IIs can then aid Rab11A positive markers to form either early endosomes or multivesicular bodies. Early endosomes can either be transported to lysosomes for degradation or be recycled back to the cell surface. If the vesicles later form multivesicular bodies, Cripto can then be secreted into the extracellular environment via exosomes to affect neighboring cells. This leads to the induction of Cripto's canonical pathways, including the phosphorylation of Smad 2/3 and then regulation of pluripotent genes at the transcriptional level (**Figure 10**).

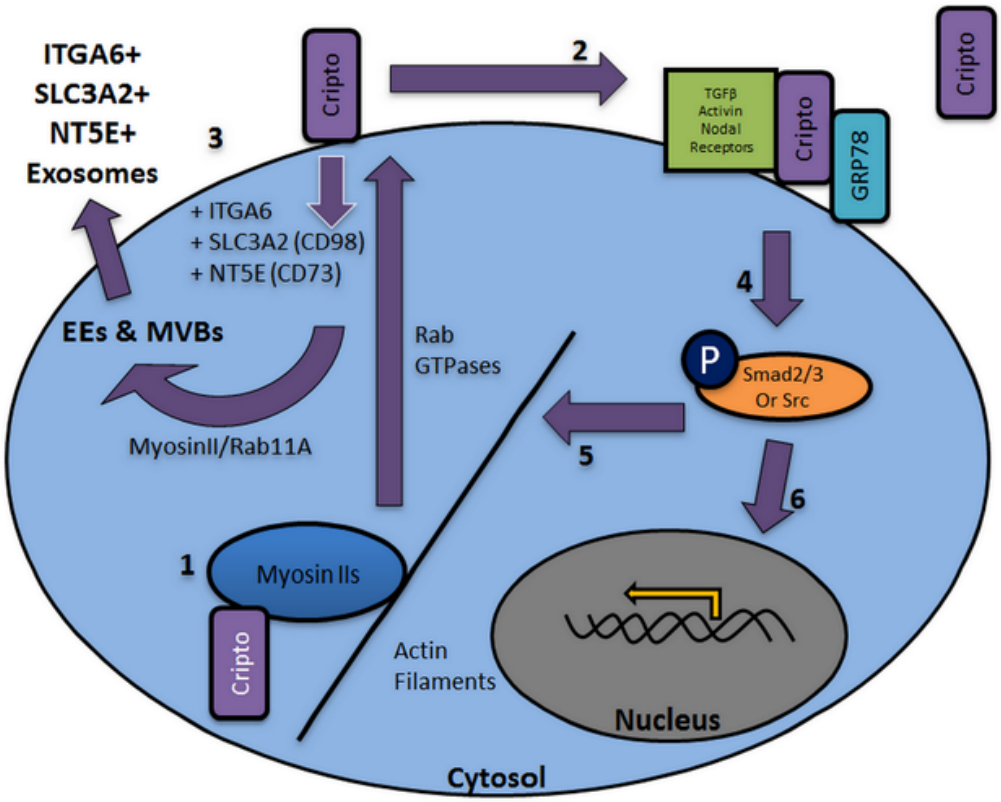

Figure 10. Proposed mechanism of Cripto and Myosin II mediated tissue regeneration. 1) Myosin II mediates transport of Cripto. 2) Cell-surface or soluble Cripto binds to receptors. 3) Endosomal/ exosome trafficking. 4) Intracellular signaling. 5) Cytoskeleton regulation. 6) Transcriptional regulation.

References

1. Gurtner, G. C., Werner, S., Barrandon, Y., & Longaker, M. T. (2008). Wound repair and regeneration. *Nature*, *453*(7193), 314–321. http://doi.org/10.1038/nature07039

2. Singer, A. J., & Clark, R. A. (1999). Cutaneous wound healing. The New England Journal of Medicine, 341(10), 738–46. http://doi.org/10.1056/NEJM199909023411006

3. Zaret, K. S., & Grompe, M. (2008). Generation and regeneration of cells of the liver and pancreas. Science (New York, N.Y.), 322(5907), 1490–4. http://doi.org/10.1126/science.1161431

4. Gehart, H., & Clevers, H. (2015). Repairing organs: Lessons from intestine and liver. Trends in Genetics. http://doi.org/10.1016/j.tig.2015.04.005

5. Nolan, C. J., Damm, P., & Prentki, M. (2011). Type 2 diabetes across generations: From pathophysiology to prevention and management. In *The Lancet* (Vol. 378, pp. 169–181). http://doi.org/10.1016/S0140-6736(11)60614-4

6. Pascual-Gil, S., Garbayo, E., Díaz-Herráez, P., Prosper, F., & Blanco-Prieto, M. J. (2015). Heart regeneration after myocardial infarction using synthetic biomaterials. Journal of Controlled Release. http://doi.org/10.1016/j.jconrel.2015.02.009

7. Poss, K. D., Keating, M. T., & Nechiporuk, A. (2003). Tales of regeneration in zebrafish. *Developmental Dynamics*. http://doi.org/10.1002/dvdy.10220

8. Raya, A., Consiglio, A., Kawakami, Y., Rodriguez-Esteban, C., & Izpisúa-Belmonte, J. C. (2004). The zebrafish as a model of heart regeneration. Cloning and Stem Cells, 6(4), 345–51. http://doi.org/10.1089/clo.2004.6.345

9. Goessling, W., & Sadler, K. C. (2015). Zebrafish: An Important Tool for Liver Disease Research. *Gastroenterology*. http://doi.org/10.1053/j.gastro.2015.08.034

10. Wan, J., & Goldman, D. (2016). Retina regeneration in zebrafish. Current Opinion in Genetics and Development. http://doi.org/10.1016/j.gde.2016.05.009

11. Tal, T. L., Franzosa, J. A., & Tanguay, R. L. (2010). Molecular signaling networks that choreograph epimorphic fin regeneration in Zebrafish - A mini-review. Gerontology. http://doi.org/10.1159/000259327

12. Fleisch, V. C., Fraser, B., & Allison, W. T. (2011). Investigating regeneration and functional integration of CNS neurons: Lessons from zebrafish genetics and other fish species. Biochimica et Biophysica Acta - Molecular Basis of Disease. http://doi.org/10.1016/j.bbadis.2010.10.012

13. Iovine, M. K. (2007). Conserved mechanisms regulate outgrowth in zebrafish fins. *Nature Chemical Biology*, *3*(10), 613–618. http://doi.org/10.1038/nchembio.2007.36

14. Nechiporuk, A., & Keating, M. T. (2002). A proliferation gradient between proximal and msxb-expressing distal blastema directs zebrafish fin regeneration. *Development (Cambridge, England)*, *129*(11), 2607–2617.

15. Akimenko, M. A., Marí-Beffa, M., Becerra, J., & Géraudie, J. (2003). Old questions, new tools, and some answers to the mystery of fin regeneration. *Developmental Dynamics*. http://doi.org/10.1002/dvdy.10248

16. Aggarwal, S., & Pittenger, M. F. (2005). Human mesenchymal stem cells modulate allogeneic immune cell responses. *Blood*, *105*(4), 1815–1822. http://doi.org/10.1182/blood-2004-04-1559

17. Gnecchi, M., Zhang, Z., Ni, A., & Dzau, V. J. (2008). Paracrine mechanisms in adult stem cell signaling and therapy. *Circulation Research*. http://doi.org/10.1161/CIRCRESAHA.108.176826

18. Hocking, A. M., & Gibran, N. S. (2010). Mesenchymal stem cells: Paracrine signaling and differentiation during cutaneous wound repair. *Experimental Cell Research*.

19. Ries, C., Egea, V., Karow, M., Kolb, H., Jochum, M., & Neth, P. (2007). MMP-2, MT1-MMP, and TIMP-2 are essential for the invasive capacity of human mesenchymal stem cells: Differential regulation by inflammatory cytokines. Blood, 109(9), 4055–4063. http://doi.org/10.1182/blood-2006-10-051060

20. Salomon, D. S., Bianco, C., Ebert, A. D., Khan, N. I., De Santis, M., Normanno, N., … Persico, G. (2000). The EGF-CFC family: Novel epidermal growth factor-related proteins in development and cancer. *Endocrine-Related Cancer*.

21. Ding, J., Yang, L., Yan, Y. T., Chen, a, Desai, N., Wynshaw-Boris, a, & Shen, M. M. (1998). Cripto is required for correct orientation of the anterior-posterior axis in the mouse embryo. *Nature*, *395*(6703), 702–707. http://doi.org/10.1038/27215

22. Li, Y., Welm, B., Podsypanina, K., Huang, S., Chamorro, M., Zhang, X., … Varmus, H. E. (2003). Evidence that transgenes encoding components of the Wnt signaling pathway preferentially induce mammary cancers from progenitor cells. *Proceedings of the National Academy of Sciences of the United States of America*, *100*(26), 15853–8. http://doi.org/10.1073/pnas.2136825100

23. Strizzi, L., Abbott, D. E., Salomon, D. S., & Hendrix, M. J. C. (2008). Potential for cripto-1 in defining stem cell-like characteristics in human malignant melanoma. Cell Cycle. http://doi.org/10.4161/cc.7.13.6236

24. Kelber, J. A., Shani, G., Booker, E. C., Vale, W. W., & Gray, P. C. (2008). Cripto is a noncompetitive activin antagonist that forms analogous signaling complexes with activin and nodal. *Journal of Biological Chemistry*, *283*(8), 4490–4500. http://doi.org/10.1074/jbc.M704960200

25. Gray, P. C., Shani, G., Aung, K., Kelber, J., & Vale, W. (2006). Cripto binds transforming growth factor beta (TGF-beta) and inhibits TGF-beta signaling. *Molecular and Cellular Biology*, *26*(24), 9268–78. http://doi.org/10.1128/MCB.01168-06

26. Yan, Y., Liu, J., Luo, Y., E, C., Haltiwanger, R. S., Abate-Shen, C., & Shen, M. M. (2002). Dual roles of Cripto as a ligand and coreceptor in the nodal signaling pathway. Molecular and Cellular Biology, 22(13), 4439–4449. http://doi.org/10.1128/MCB.22.13.4439-4449.2002

27. Miharada, K., Karlsson, G., Rehn, M., Rörby, E., Siva, K., Cammenga, J., & Karlsson, S. (2011). Cripto regulates hematopoietic stem cells as a hypoxic-niche-related factor through cell surface receptor GRP78. Cell Stem Cell, 9(4), 330–344. http://doi.org/10.1016/j.stem.2011.07.016

28. Kelber, J. a, Panopoulos, a D., Shani, G., Booker, E. C., Belmonte, J. C., Vale, W. W., & Gray, P. C. (2009). Blockade of Cripto binding to cell surface GRP78 inhibits oncogenic Cripto signaling via MAPK/PI3K and Smad2/3 pathways. *Oncogene*, *28*(24), 2324–36. http://doi.org/10.1038/onc.2009.97

29. Wylie, S. R., Wu, P. -j., Patel, H., & Chantler, P. D. (1998). A conventional myosin motor drives neurite outgrowth. Proceedings of the National Academy of Sciences, 95(22), 12967–12972. http://doi.org/10.1073/pnas.95.22.12967

30. Wang, F. S., Wolenski, J. S., Cheney, R. E., Mooseker, M. S., & Jay, D. G. (1996). Function of myosin-V in filopodial extension of neuronal growth cones. *Science (New York, N.Y.)*, *273*(5275), 660–663. http://doi.org/10.1126/science.273.5275.660

31. Anderson, S. M., Yu, G., Giattina, M., & Miller, J. L. (1996). Intercellular transfer of a glycosylphosphatidylinositol (GPI)-linked protein: release and uptake of CD4-GPI from recombinant adeno-associated virus-transduced HeLa cells. *Proceedings of the National Academy of Sciences of the United States of America*, *93*(12), 5894–8. http://doi.org/10.1073/pnas.93.12.5894

32. Simons, M., & Raposo, G. (2009). Exosomes--vesicular carriers for intercellular communication. Current Opinion in Cell Biology, 21, 575–581. http://doi.org/10.1016/j.ceb.2009.03.007

33. Gerdes, H. H., & Carvalho, R. N. (2008). Intercellular transfer mediated by tunneling nanotubes. *Current Opinion in Cell Biology*. http://doi.org/10.1016/j.ceb.2008.03.005

34. Eisfeld, A. J., Kawakami, E., Watanabe, T., Neumann, G., & Kawaoka, Y. (2011). RAB11A Is Essential for Transport of the Influenza Virus Genome to the Plasma Membrane. Journal of Virology, 85(13), 6117–6126. http://doi.org/10.1128/jvi.00378-11

35. Lapierre, L. A., Ducharme, N. A., Drake, K. R., Goldenring, J. R., & Kenworthy, A. K. (2012). Coordinated regulation of caveolin-1 and Rab11A in apical recycling compartments of polarized epithelial cells. Experimental Cell Research, 318(2), 103–113. http://doi.org/10.1016/j.yexcr.2011.10.010

36. Nakamura, Y. (Nakamura et al., 2015)(Nakamura et al., 2015)Nakamura, Y., Miyaki, S., Ishitobi, H., Matsuyama, S., Nakasa, T., Kamei, N., … Ochi, M. (2015). Mesenchymal-stem-cell-derived exosomes accelerate skeletal muscle regeneration. *FEBS Letters*, *589*(11), 1257–1265. http://doi.org/10.1016/j.febslet.2015.03.031

37. M. a Akimenko, S. L. Johnson, M. Westerfield, and M. Ekker, "Differential induction of four msx homeobox genes during fin development and regeneration in zebrafish.," *Development*, vol. 121, pp. 347–357, 1995.

38. J. P. Concordet, K. E. Lewis, J. W. Moore, L. V Goodrich, R. L. Johnson, M. P. Scott, and P. W. Ingham, "Spatial regulation of a zebrafish patched homologue reflects the roles of sonic hedgehog and protein kinase A in neural tube and somite patterning," *Development*, vol. 122, no. 9, pp. 2835–2846, 1996.

39. A. DeLaurier, B. Frank Eames, B. Blanco-Sánchez, G. Peng, X. He, M. E. Swartz, B. Ullmann, M. Westerfield, and C. B. Kimmel, "Zebrafish sp7:EGFP: A transgenic for studying otic vesicle formation, skeletogenesis, and bone regeneration," *Genesis*, vol. 48, no. 8, pp. 505–511, 2010.

40. N. Lawson and B. Weinstein, "In vivo imaging of embryonic vascular development using transgenic zebrafish," *Dev. Biol.*, vol. 248, no. 2, pp. 307–18, 2002.

41. J. Zou, F. Beermann, J. Wang, K. Kawakami, and X. Wei, "The Fugu tyrp1 promoter directs specific GFP expression in zebrafish: Tools to study the RPE and the neural crest-derived melanophores," *Pigment Cell Res.*, vol. 19, no. 6, pp. 615–627, 2006.

42. B. T. Spike, J. A. Kelber, E. Booker, M. Kalathur, R. Rodewald, J. Lipianskaya, J. La, M. He, T. Wright, R. Klemke, G. M. Wahl, and P. C. Gray, "CRIPTO/GRP78 signaling maintains fetal and adult mammary stem cells ex vivo," *Stem Cell Reports*, vol. 2, no. 4, pp. 427–439, 2014.

43. G. Minchiotti, S. Parisi, G. Liguori, M. Signore, G. Lania, E. D. Adamson, C. T. Lago, and M. G. Persico, "Membrane-anchorage of Cripto protein by glycosylphosphatidylinositol and its distribution during early mouse development," *Mech. Dev.*, vol. 90, no. 2, pp. 133–142, 2000.

44. J. Chu, J. Ding, K. Jeays-Ward, S. M. Price, M. Placzek, and M. M. Shen, "Non-cell-autonomous role for Cripto in axial midline formation during vertebrate embryogenesis.," *Development*, vol. 132, no. 24, pp. 5539–51, 2005.

45. E. Ikonen, J. B. de Almeid, K. R. Fath, D. R. Burgess, K. Ashman, K. Simons, and J. L. Stow, "Myosin II is associated with Golgi membranes: identification of p200 as nonmuscle myosin II on Golgi-derived vesicles.," *J. Cell Sci.*, vol. 110 (Pt 1, pp. 2155–2164, 1997.

46. G. Shani, W. H. Fischer, N. J. Justice, J. A. Kelber, W. Vale, and P. C. Gray, "GRP78 and Cripto form a complex at the cell surface and collaborate to inhibit transforming growth factor beta signaling and enhance cell growth.," Mol. Cell. Biol., vol. 28, no. 2, pp. 666–77, 2008.

47. Kim, J. M., Lee, S. T., Chu, K., Jung, K. H., Song, E. C., Kim, S. J., … Roh, J. K. (2007). Systemic transplantation of human adipose stem cells attenuated cerebral inflammation and degeneration in a hemorrhagic stroke model. *Brain Research*, *1183*(1), 43–50. http://doi.org/10.1016/j.brainres.2007.09.005

48. Amado, L. C., Saliaris, A. P., Schuleri, K. H., St. John, M., Xie, J.-S., Cattaneo, S., … Hare, J. M. (2005). Cardiac repair with intramyocardial injection of allogeneic mesenchymal stem cells after myocardial infarction. *Proceedings of the National Academy of Sciences*, *102*(32), 11474–11479. http://doi.org/10.1073/pnas.0504388102

49. Lu, D., Chen, B., Liang, Z., Deng, W., Jiang, Y., Li, S., … Chen, S. (2011). Comparison of bone marrow mesenchymal stem cells with bone marrow-derived mononuclear cells for treatment of diabetic critical limb ischemia and foot ulcer: A double-blind, randomized, controlled trial. *Diabetes Research and Clinical Practice*, *92*(1), 26–36. http://doi.org/10.1016/j.diabres.2010.12.010

50. Gray, P. C., & Vale, W. (2012). Cripto/GRP78 modulation of the TGF-?? pathway in development and oncogenesis. *FEBS Letters*. http://doi.org/10.1016/j.febslet.2012.01.051

51. Watanabe, K., Bianco, C., Strizzi, L., Hamada, S., Mancino, M., Bailly, V., … Salomon, D. S. (2007). Growth factor induction of cripto-1 shedding by glycosylphosphatidylinositol-phospholipase D and enhancement of endothelial cell migration. *Journal of Biological Chemistry*, *282*(43), 31643–31655. http://doi.org/10.1074/jbc.M702713200

52. Caplan, A. I., & Dennis, J. E. (2006). Mesenchymal stem cells as trophic mediators. *Journal of Cellular Biochemistry*. http://doi.org/10.1002/jcb.20886

53. Xu, G., Zhang, Y., Zhang, L., Ren, G., & Shi, Y. (2007). The role of IL-6 in inhibition of lymphocyte apoptosis by mesenchymal stem cells. *Biochemical and Biophysical Research Communications*, *361*(3), 745–750. http://doi.org/10.1016/j.bbrc.2007.07.052

54. Crisostomo, P. R., Wang, Y., Markel, T. A., Wang, M., Lahm, T., & Meldrum, D. R. (2008). Human mesenchymal stem cells stimulated by TNF-alpha, LPS, or hypoxia produce growth factors by an NF kappa B- but not JNK-dependent mechanism. *American Journal of Physiology. Cell Physiology*, *294*(3), C675–82. http://doi.org/10.1152/ajpcell.00437.2007

55. Uccelli, A., Moretta, L., & Pistoia, V. (2008). Mesenchymal stem cells in health and disease. *Nature Reviews. Immunology*, *8*(9), 726–736. http://doi.org/10.1038/nri2395

56. Han, Z., Jing, Y., Zhang, S., Liu, Y., Shi, Y., & Wei, L. (2012). The role of immunosuppression of mesenchymal stem cells in tissue repair and tumor growth. *Cell & Bioscience*, *2*(1), 8. http://doi.org/10.1186/2045-3701-2-8

57. Bianchi, G., Borgonovo, G., Pistoia, V., & Raffaghello, L. (2011). Immunosuppressive cells and tumour microenvironment: Focus on mesenchymal stem cells and myeloid derived suppressor cells. *Histology and Histopathology*.

58. Prockop, D. (1997). Marrow stromal cells as stem cells for nonhematopoietic tissues. *Science*, *267*, 71–74. http://doi.org/10.4415/ANN_11_04_04

59. Salem, H. K., & Thiemermann, C. (2010). Mesenchymal stromal cells: Current understanding and clinical status. *Stem Cells*. http://doi.org/10.1002/stem.269

60. Dezawa, M., Ishikawa, H., Itokazu, Y., Yoshihara, T., Hoshino, M., Takeda, S., … Nabeshima, Y. (2005). Bone marrow stromal cells generate muscle cells and repair muscle degeneration. *Science (New York, N.Y.)*, *309*(5732), 314–7. http://doi.org/10.1126/science.1110364

61. Tarte, K., Gaillard, J., Lataillade, J. J., Fouillard, L., Becker, M., Mossafa, H., … Sensebé, L. (2010). Clinical-grade production of human mesenchymal stromal cells: Occurrence of aneuploidy without transformation. *Blood*, *115*(8), 1549–1553. http://doi.org/10.1182/blood-2009-05-219907

62. Bocelli-Tyndall, C., Zajac, P., Di Maggio, N., Trella, E., Benvenuto, F., Iezzi, G., … Tyndall, A. (2010). Fibroblast growth factor 2 and platelet-derived growth factor, but not platelet lysate, induce proliferation-dependent, functional class II major histocompatibility complex antigen in human mesenchymal stem cells. *Arthritis and Rheumatism*, *62*(12), 3815–3825. http://doi.org/10.1002/art.27736

63. Smith, A., Avaron, F., Guay, D., Padhi, B. K., & Akimenko, M. A. (2006). Inhibition of BMP signaling during zebrafish fin regeneration disrupts fin growth and scleroblast differentiation and function. *Developmental Biology*, *299*(2), 438–454. http://doi.org/10.1016/j.ydbio.2006.08.016

64. Laforest, L., Brown, C. W., Poleo, G., Géraudie, J., Tada, M., Ekker, M., & Akimenko, M. a. (1998). Involvement of the sonic hedgehog, patched 1 and bmp2 genes

in patterning of the zebrafish dermal fin rays. *Development (Cambridge, England)*, *125*(21), 4175–4184.

65. Quint, E., Smith, A., Avaron, F., Laforest, L., Miles, J., Gaffield, W., & Akimenko, M. A. (2002). Bone patterning is altered in the regenerating zebrafish caudal fin after ectopic expression of sonic hedgehog and bmp2b or exposure to cyclopamine. *Proc Natl Acad Sci U S A*, *99*(13), 8713–8718. http://doi.org/10.1073/pnas.122571799

66. Aykul, S., Parenti, A., Chu, KY., Reske, J., Floer, M., Ralston, A., Martinez-Hackert, E. (2017). Biochemical and Cellular Analysis Reveals Ligand Binding Specificities, a Molecular Basis for Ligand Recognition, and Membrane Association-dependent Activities of Cripto-1 and Cryptic. J Biol Chem. 2017 Mar 10;292(10):4138-4151. doi: 10.1074/jbc.M116.747501.

67. Blanchet, M.-H., Le Good, J. A., Oorschot, V., Baflast, S., Minchiotti, G., Klumperman, J., & Constam, D. B. (2008). Cripto localizes Nodal at the limiting membrane of early endosomes. *Science Signaling*, *1*(45), ra13. http://doi.org/10.1126/scisignal.1165027

68. Gormal, R. S., Nguyen, T. H., Martin, S., Papadopulos, A., & Meunier, F. a. (2015). An Acto-Myosin II Constricting Ring Initiates the Fission of Activity-Dependent Bulk Endosomes in Neurosecretory Cells. *Journal of Neuroscience*, *35*(4), 1380–1389. http://doi.org/10.1523/JNEUROSCI.3228-14.2015

69. Samaniego, R., Sánchez-Martín, L., Estecha, A., & Sánchez-Mateos, P. (2007). Rho/ROCK and myosin II control the polarized distribution of endocytic clathrin structures at the uropod of moving T lymphocytes. *Journal of Cell Science*, *120*(Pt 20), 3534–43. http://doi.org/10.1242/jcs.006296

70. Wang, X., Kumar, R., Navarre, J., Casanova, J. E., & Goldenring, J. R. (2000). Regulation of vesicle trafficking in Madin-Darby canine kidney cells by Rab11A and Rab25. *Journal of Biological Chemistry*, *275*(37), 29138–29146. http://doi.org/10.1074/jbc.M004410200

71. Savina, A., Fader, C. M., Damiani, M. T., & Colombo, M. I. (2005). Rab11 promotes docking and fusion of multivesicular bodies in a calcium-dependent manner. *Traffic*, *6*(2), 131–143. http://doi.org/10.1111/j.1600-0854.2004.00257.x

72. Yashiro, H., Loza, A. J., Skeath, J. B., & Longmore, G. D. (2014). Rho1 regulates adherens junction remodeling by promoting recycling endosome formation through activation of myosin II. *Molecular Biology of the Cell*, *25*(19), 2956–69. http://doi.org/10.1091/mbc.E14-04-0894

73. Plosa, E. J., Gooding, K. A., Zent, R., & Prince, L. S. (2012). Nonmuscle myosin II regulation of lung epithelial morphology. *Developmental Dynamics : An Official Publication of the American Association of Anatomists*, *241*(11), 1770–81.

http://doi.org/10.1002/dvdy.23866